

Ground Cloud Dispersion Measurements During the Titan IV Mission #K16 (24 April 1996) at Cape Canaveral Air Force Station

Volume 2—Further Analysis of Quantitative Imagery
and of Aircraft HCI Data

3 April 2000

Prepared by

R. N. ABERNATHY and K. L. FOSTER
Space Science Applications Laboratory
Laboratory Operations

Prepared for

SPACE AND MISSILE SYSTEMS CENTER
AIR FORCE MATERIEL COMMAND
2430 E. El Segundo Boulevard
Los Angeles Air Force Base, CA 90245

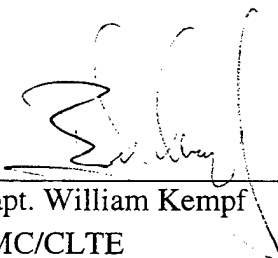
Space Systems Group

APPROVED FOR PUBLIC RELEASE;
DISTRIBUTION UNLIMITED

This report was submitted by The Aerospace Corporation, El Segundo, CA 90245-4691, under Contract No. F04701-93-C-0094 with the Space and Missile Systems Center, 2430 E. El Segundo Blvd., Los Angeles Air Force Base, CA 90245. It was reviewed and approved for The Aerospace Corporation by A. B. Christensen, Principal Director, Space Science Applications Laboratory; and N. F. Dowling, Director, Environmental Systems, Systems Engineering Directorate. Capt. W. Kempf was the project officer.

This report has been reviewed by the Public Affairs Office (PAS) and is releasable to the National Technical Information Service (NTIS). At NTIS, it will be available to the general public, including foreign nationals.

This technical report has been reviewed and is approved for publication. Publication of this report does not constitute Air Force approval of the report's findings or conclusions. It is published only for the exchange and stimulation of ideas.



Capt. William Kempf
SMC/CLTE

REPORT DOCUMENTATION PAGE			Form Approved OMB No. 0704-0188	
Public reporting burden for this collection of information is estimated to average 1 hour per response, including the time for reviewing instructions, searching existing data sources, gathering and maintaining the data needed, and completing and reviewing the collection of information. Send comments regarding this burden estimate or any other aspect of this collection of information, including suggestions for reducing this burden to Washington Headquarters Services, Directorate for Information Operations and Reports, 1215 Jefferson Davis Highway, Suite 1204, Arlington, VA 22202-4302, and to the Office of Management and Budget, Paperwork Reduction Project (0704-0188), Washington, DC 20503.				
1. AGENCY USE ONLY (Leave blank)		2. REPORT DATE 3 April 2000		3. REPORT TYPE AND DATES COVERED
4. TITLE AND SUBTITLE Ground Cloud Dispersion Measurements During the Titan IV Mission #K16 (24 April 1996) at Cape Canaveral Air Force Station			5. FUNDING NUMBERS F04701-93-C-0094	
6. AUTHOR(S) R. N. Abernathy and K. L. Foster				
7. PERFORMING ORGANIZATION NAME(S) AND ADDRESS(ES) The Aerospace Corporation Laboratory Operations El Segundo, CA 90245-4691			8. PERFORMING ORGANIZATION REPORT NUMBER TR-2000(1490)-1	
9. SPONSORING/MONITORING AGENCY NAME(S) AND ADDRESS(ES) Space and Missile Systems Center Air Force Materiel Command 2430 E. El Segundo Boulevard Los Angeles Air Force Base, CA 90245			10. SPONSORING/MONITORING AGENCY REPORT NUMBER SMC-TR-00-08	
11. SUPPLEMENTARY NOTES				
12a. DISTRIBUTION/AVAILABILITY STATEMENT Approved for public release; distribution unlimited			12b. DISTRIBUTION CODE	
13. ABSTRACT (Maximum 200 words) <p>A previous report presented an overview and data summary for ground cloud dispersion measurements during the Titan IV mission #K16 launch from CCAFS on 24 April 1996. That report documented the instrumentation, methods of analysis, and preliminary results for the program. The preliminary results included the following: (1) the imagery-derived cloud speed, direction, and position for the first 6 min after launch; (2) summary plots of the aircraft-derived HCl data for the first 88 min after launch; and (3) comparison of imagery-derived, aircraft-derived, rawinsonde-derived data to REEDM version 7.07 predictions. This second report provides a detailed comparison of the imagery-derived extent of the ground cloud to simultaneous aircraft sampling data. The combined data provides a three-dimensional perspective of the exhaust cloud during the first 6 min after launch. In addition, this report includes a more detailed graphing and analysis of the aircraft's HCl measurements.</p> <p>The #K16 imagery and aircraft data documented substantial differences between measured and T-0.7 h REEDM version 7.07 predictions. According to the quantitative visible imagery from UCS-7 and Press sites, the cloud took 3.5 min to stabilize (20% faster than predicted), stabilized at 1023m in altitude (35% higher than predicted), moved in a south-southwesterly direction (versus the east-southeasterly prediction), and moved at an average speed of 3.6 m/s (38% slower than predicted). Comparison of the aircraft's HCl measurements to the visible extent of the cloud revealed consistent edge detection by both methods. The aircraft's HCl measurements also confirmed the imagery-derived bearing for the lower lobe of the ground cloud and were consistent with the observed high-altitude wind shear to the east.</p>				
14. SUBJECT TERMS Titan IV, Solid Rocket Motor, Launch Cloud, Ground Cloud, Exhaust Cloud, Dispersion, Tracking, Imagery, Hydrochloric Acid, HCl, Aircraft, Sampling, Model Validation, MVP, Model Validation Program, Geomet			15. NUMBER OF PAGES 44	
			16. PRICE CODE	
17. SECURITY CLASSIFICATION OF REPORT UNCLASSIFIED	18. SECURITY CLASSIFICATION OF THIS PAGE UNCLASSIFIED	19. SECURITY CLASSIFICATION OF ABSTRACT UNCLASSIFIED	20. LIMITATION OF ABSTRACT	

Acknowledgments

The Air Force Space and Missile Systems Center's Launch Programs Office (SMC/CL) is sponsoring the Atmospheric Dispersion Model Validation Program (MVP). This program is collecting launch cloud dispersion data that will be used to determine the accuracy of atmospheric dispersion models, such as REEDM, in predicting toxic hazard corridors at the launch ranges. This report correlates quantitative launch cloud imagery with aircraft HCl measurements performed during the Titan IV Mission #K16 at Cape Canaveral Air Force Station on 24 April 1996.

An MVP Integrated Product Team (IPT) led by Capt. Bill Kempf (SMC/CLTO) is directing the MVP effort. Dr. Bart Lundblad of The Aerospace Corporation's Environmental Systems Directorate (ESD) is the MVP technical manager.

Visible imagery measurements of the launch cloud were made by Dr. Robert N. Abernathy, Ms. Karen L. Foster, and Ms. J. Y. Webb of The Aerospace Corporation's Surveillance Technology Department (STD). Mr. John Ligda, Mr. Kent Evans, and Mr. James Beardall of The Aerospace Corporation's Eastern Range Directorate and Dr. Bart Lundblad provided field assistance. Mr. Doug Schulthess of The Aerospace Corporation's Eastern Range Directorate coordinated site selection and logistical support with Range organizations. Ms. Foster digitized imagery data for analysis by Dr. Abernathy. Mr. Kasper created and maintains the PLMTRACK program used by Dr. Abernathy for pair-wise analysis of simultaneously acquired imagery from two sites. Ms. Foster performed the graphical comparison of the imagery results against the aircraft HCl measurements. Dr. Abernathy prepared the description of the cloud imagery results and analysis.

The aircraft-based HCl measurement effort was managed by Mr. Marv Becker and Mr. Pete Mazur of SRS Technologies. The Piper Seminole sampling aircraft was owned and operated by Florida Institute of Technology. The aircraft was outfitted with a Geomet HCl detector that was modified and calibrated for airborne sampling by Mr. Paul Yocom of the NASA Toxic Vapor Detection/Contamination Monitoring Laboratory. Ms. Jeanne Hawkins of the 45th Medical Group Bioenvironmental Engineering Services (45 AMDS/SGPB) was on-board the aircraft during the sampling measurements to monitor Geomet performance and cockpit contamination. The on-board data logger and GPS system were provided and installed by Mr. Shane Beard of NOAA's Environmental Research Laboratories. The raw Geomet HCl detector data were processed and analyzed by Dr. Abernathy and Ms. Foster. Ms. Foster performed the graphical comparison of the imagery results against the aircraft HCl measurements. Dr. Abernathy analyzed the response characteristics and calibration of the Geomet. Dr. Abernathy prepared the description of the aircraft sampling and cloud imagery results.

The meteorological data displayed in this report were provided by Mr. Randy Evans of the NASA Applied Meteorology Unit and ENSCO, Inc.

Contents

Executive Summary	ix
1. Introduction	1
1.1 Model Validation Program	1
1.2 #K16 Ground Cloud Measurements	2
1.2.1 Previously Reported Results of Quantitative Imagery	3
1.2.2 Previously Reported Results of Aircraft HCI Measurements	3
1.2.3 Additional Analysis Included in This Report	4
2. Analysis	5
2.1 Linear Interpretation of Imagery	5
2.2 PLMTRACK Analysis of Imagery from Two Sites	6
2.3 Geomet HCI Measurements	7
2.3.1 Reference for Altitudes	8
2.3.2 Geomet Calibration Data	8
2.3.3 Geomet Response Characteristics	8
2.3.3.1 Accurate Integrated HCI Dose	8
2.3.3.2 Accurate Edge Detection and Peak Location Reporting	9
3. Results	11
3.1 Comparison of Aircraft HCI Profiles to Imaged Ground Cloud Extent	11
3.1.1 Cartesian Extent of the Ground Cloud for Passes 1-3	11
3.1.2 Average HCI Concentration and Total HCI Dosage for Passes 1-9	14
3.1.3 Aircraft Altitude and Imagery-Derived Vertical Extent for Passes 1-4	21
3.2 Detailed Plots of Aircraft-Derived HCI Profiles (10-min Intervals)	22
3.3 Summary Plots of Aircraft Geomet HCI Data (88 minute Interval)	24
4. Conclusions	29
References	31

Appendix A—Acronyms and Abbreviations	33
Appendix B—10-Min Plots for Aircraft Data.....	35

Figures

1. PLMTRACK box method within an image and projected onto ground plane.....	6
2. PLMTRACK ray tracing and extent of #K16 exhaust cloud (T+ 4.0 min).....	7
3. Imagery- and aircraft-derived Cartesian extent for K16 cloud (T=3-7.4 min).	12
4. Pass 1 (T=0-4.5 min) versus imagery-derived polygon (T=3-4 min).	12
5. Pass 2 (T=4.5-5.8 min) versus imagery-derived polygon (T=5 min).....	13
6. Pass 3 (T=5.8-7.4 min) versus imagery-derived polygons (T=6 min).	13
7. Visible image of ground cloud (T+5.0 min) from UCS-7 site.	15
8. Visible image of the ground cloud (T+5.0 min) from Press site.....	15
9. Pass 1 (T=3.4-4.7 min) HCl concentration and dosage data.	16
10. Pass 2 (T=4.7-6.3 min) HCl concentration and dosage data.	16
11. Pass 3 (T=6.3-8.0 min) HCl concentration and dosage data.	17
12. Pass 4 (T=8.2-10 min) HCl concentration and dosage data.	17
13. Pass 5 (T=10.6-12 min) HCl concentration and dosage data.	18
14. Pass 6 (T=12.2-13.5 min) HCl concentration and dosage data.	18
15. Pass 7 (T=13.9-15.5 min) HCl concentration and dosage data.	19
16. Pass 8 (T=16.3-18.3 min) HCl concentration and dosage data.	19
17. Pass 9 (T=18.5-20.5 min) HCl concentration and dosage data.	20
18. Altitude plot for aircraft and exhaust cloud (T = 0 to 10 min) with HCl Data.	22
19. Cartesian position labeled with HCl concentration (0 to 90 min).....	25
20. Polar angle and HCl concentration plotted against time (0 to 90 min).	25
21. Ground Distance and HCl concentration plotted against time (0 to 90 min).	26

22. Altitude and HCl concentration plotted against time (0 to 90 min).....	26
23. Effective speed and HCl concentration plotted against time (0 to 90 min).....	27
B-1. Time and Cartesian Plots for Passes 1-4 (T = 0 to 10 minutes).....	36
B-2. Time and Cartesian Plots for Passes 5-9 (T = 10 to 20 minutes).....	37
B-3. Time and Cartesian Plots for Passes 10-13 (T = 20 to 30 minutes).....	38
B-4. Time and Cartesian Plots for Passes 14-18 (T = 30 to 40 minutes).....	39
B-5. Time and Cartesian Plots for Passes 19-22 (T = 40 to 50 minutes).....	40
B-6. Time and Cartesian Plots for Passes 23-25 (T = 50 to 60 minutes).....	41
B-7. Time and Cartesian Plots for Passes 26-30 (T = 60 to 70 minutes).....	42
B-8. Time and Cartesian Plots for Passes 31-35 (T = 70 to 80 minutes).....	43
B-9. Time and Cartesian Plots for Pass 36 and Runway (T = 80 to 88 minutes).	44

Tables

1. Summary of HCl Concentration Data for Passes 1-9.	20
2. Summary of Aircraft-Derived Ground Cloud Information.....	23

Executive Summary

A previous report presented an overview and data summary for ground cloud dispersion measurements during the Titan IV mission #K16 launch from CCAFS on 24 April 1996. That report documented the instrumentation, methods of analysis, and preliminary results for the program. The preliminary results included the following: (1) the imagery-derived cloud speed, direction, and position for the first 6 min after launch; (2) summary plots of the aircraft-derived HCl data for the first 88 min after launch; and (3) comparison of imagery-derived, aircraft-derived, rawinsonde-derived data to REEDM version 7.07 predictions. This second report provides a detailed comparison of the imagery-derived extent of the ground cloud to simultaneous aircraft sampling data. The combined data provides a three-dimensional perspective of the exhaust cloud during the first 6 min after launch. In addition, this report includes a more detailed graphing and analysis of the aircraft's HCl measurements.

The #K16 imagery and aircraft data documented substantial differences between measured and T-0.7 h REEDM version 7.07 predictions. According to the quantitative visible imagery from UCS-7 and Press sites, the cloud took 3.5 min to stabilize (20% faster than predicted), stabilized at 1023 m in altitude (35% higher than predicted), moved in a south-southwesterly direction (versus the east-southeasterly prediction), and moved at an average speed of 3.6 m/s (38% slower than predicted). Comparison of the aircraft's HCl measurements to the visible extent of the cloud revealed consistent edge detection by both methods. The aircraft's HCl measurements also confirmed the imagery-derived bearing for the lower lobe of the ground cloud and were consistent with the observed high-altitude wind shear to the east.

The analyzed data for the Titan IV mission #K16 is one part of a larger dataset. Dispersion models must account for many variables that include the following: the effect of terrain (i.e., Eastern and Western launch ranges); weather conditions (i.e., wind speed, wind shear, cloud cover, humidity, rain); daily variations (i.e., solar angle and sea breeze conditions); and seasonal variations (i.e., solar angle and meteorology). Therefore, the MVP acquired ground cloud dispersion data at both ranges, at various times of day (and night), and during various seasons. The #K16 deployment was the sixth of 13 Titan IV missions for which useable launch cloud dispersion data were collected by the MVP. The #K16 mission was the third of four Titan IV launches to employ an aircraft to collect HCl dispersion data. These data are being used to test dispersion models and have already been the motivation for several modifications to the REEDM.

1. Introduction

Dispersion model predictions have delayed launches from both Cape Canaveral Air Force Station (CCAFS) and Vandenberg Air Force Base (VAFB). Delays occur when the predicted concentrations of toxic gases resulting from a normal or an aborted launch exceed public exposure criteria. The Rocket Exhaust Effluent Dispersion Model (REEDM) predicts the downwind concentrations of toxic gases for various launch vehicles (e.g., Shuttle, Titan, and Delta) for the normal and several abort scenarios. REEDM predictions are deliberately conservative to compensate for uncertainties in the modeling physics. Therefore, it is desirable to validate the performance of such dispersion models against actual launch cloud dispersion and transport data.

The Air Force launch range safety organizations of the 45th Space Wing at Patrick Air Force Base (45 SW/SE) and the 30th Space Wing at VAFB (30 SW/SE) are responsible for assuring that launches are carried out only when meteorological conditions are such that nearby communities cannot be exposed to hazardous levels of HCl, the hydrazine fuels, or N_2O_4/NO_2 . Predictions of toxic hazard corridors (THCs) that extend into public areas can lead to costly launch delays. Presently, safety concerns mandate a conservative interpretation of model predictions since the models have not been fully validated. Thus, development and validation of accurate atmospheric dispersion models is expected to increase launch opportunities and thereby reduce launch costs.

1.1 Model Validation Program

The Space and Missile System Center's Launch Programs Office (SMC/CLNER) established the Atmospheric Dispersion Model Validation Program (MVP). MVP is collecting the data necessary to determine the accuracy of current and future atmospheric dispersion and chemical kinetic models in predicting THCs during launches of Titan and other vehicles at CCAFS and VAFB.

Model validation requires a complete set of cloud dispersion and transport data as well as any ancillary data needed as input to current or future dispersion models. Therefore, the MVP effort involves not only the collection of launch cloud data (i.e., HCl concentration profiles, cloud rise rates, cloud expansion rates, cloud speed, and cloud direction) but also the collection of meteorological data (i.e., rawinsonde soundings, Doppler acoustic sounder profiles, solar radiance data, terrain maps, and meteorological tower data). In addition to monitoring launch clouds, MVP involves measurements against tracer gas releases that provide not only a better definition of the source term (i.e., release altitude and geometry) but also optimization of the dataset (i.e., release conditions can be tuned for maximum overlap with sensor systems or with target land masses). Therefore, the MVP data will provide the needed test cases to validate current and future dispersion, transport, and chemical kinetic models.

The Aerospace Corporation has been deploying visible and/or IR imaging systems to Titan IV launches since the #K10 launch on 07 February 1994. The deployments in behalf of the MVP include Titan IV missions #K02, #K07, #K09, #K10, #K13, #K14, #K15, #K16, #A17, #A18, #K19,

#K21, #K22, #K23, #B24, and #B33. Typically, two-dimensional cloud images are recorded at each of two to three imaging sites and are combined in a pair-wise fashion to produce stereoscopic 3-D information about the exhaust cloud. When atmospheric conditions were favorable and two (or more) imagery sites were manned (i.e., #K02, #K07, #K13, #K15, #K16, #A17, #A18, #K19, #K21, #K22, #K23, #B24, and #B33), the analysis of these data yields the ground cloud's rise time, stabilization height, dimensions, ground track, and ground speed. These imagery data and the resulting cloud characteristics are available to modelers as part of the MVP.^{1,4}

The MVP has deployed aircraft to collect HCl concentration data for Titan IV launches #K23,¹ #K15,⁴ #K16,⁵ and #K22.⁶ Typically, the aircraft's near-field HCl concentration profiles are interpreted using the simultaneously acquired imagery. The combined data^{13,14} provide a 3-D perspective of the cloud by documenting the portion of the cloud sampled by the aircraft based upon the imagery-derived extent of the cloud and the concentration profile within that portion of the cloud. At later times, the aircraft's HCl concentration profiles^{14,15} document the trajectory followed by the cloud and the decrease in peak HCl concentration as it moves away from the range. These aircraft HCl concentration data are available to modelers as part of the MVP.^{1,4,5,6,13-15}

The MVP has not limited itself to normal launches of Titan IVs. As part of the MVP, a review¹⁶ of the 34D-9 abort cloud imagery provided an estimate of its entrainment coefficient. This datum allowed comparison of abort cloud data to normal Titan IV launch cloud data. This comparison revealed identical rates of entrainment for both scenarios. Another MVP effort¹⁷ involved the release of tracer gas from an airship (i.e., a blimp). These elevated releases enable collection of dispersion data under a variety of conditions that were not included in the normal launch scenarios. These tracer dispersion measurements involved imagery and remote detection (i.e., ground-based and aircraft) of the tracer as well as extensive meteorological data collection. Hence, the MVP will provide a multitude of data needed to validate both current and future dispersion models.

1.2 #K16 Ground Cloud Measurements

The Titan IV #K16 mission was launched successfully from the Eastern Range (i.e., from SLC-41) at 19:37 EDT (23:37 GMT) on 24 April 1996. Personnel from The Aerospace Corporation deployed three complete platforms of the Titan IV-dedicated Visible and Infrared Imaging System (VIRIS). For the #K16 early evening launch, three imagery sites recorded quantitative visible exhaust cloud imagery during the 55 min immediately following the launch. The imagery sites chosen for the #K16 launch were UCS-7 (north-northwest of SLC-41), SLC-34 blockhouse (south-southeast of SLC-41), and the Press Site (east of SLC-41). These same sites were employed for the earlier launches of Titan IV #K23 and #K19. A modified Geomet total hydrochloric acid (HCl) detector was mounted in the nose of a Piper (PA-44-180) Seminole, twin-engine, four-seat aircraft. The Geomet measured the combined aerosol and gaseous HCl concentration during the first 88 min after the #K16 launch. This aircraft sampling campaign involved Air Force, NASA, NOAA, and contractor (I-NET and SRS) organizations. The Aerospace Corporation analyzed the aircraft's HCl concentration data and the ground-based imagery as described in a previous report.⁵

Analysis of the quantitative imagery yielded the stabilization time, the stabilization height, the speed, and the trajectory of the "ground cloud" without recourse to additional data sources. The ground cloud is defined as the lower and more concentrated portion of the rocket's exhaust cloud that can

diffuse to the ground. The "launch column" is defined as the trail of the rapidly moving rocket that extends above the more spherical ground cloud.

Rawinsonde wind data were used to run "normal launch" REEDM predictions that were compared to the imagery-derived results. The REEDM predictions were documented in Appendix A of the previous report.⁵ The rawinsonde pre-launch meteorology data were documented in Appendix B of the previous report.⁵

The imagery documented a huge wind shear between the upper and lower portions of the ground cloud. This caused the ground cloud to overfill the field of view of the imagers within 6 min of launch even though the imagers continued to pan the extent of the ground cloud until 55 min after launch. Hardware failure at the SLC-34 imaging site prevented the quantitative use of its imagery. Quantitative analysis of the visible imagery from the two fully functional sites for the first 6 min after launch documented the cloud's rise time, stabilization height, trajectory, and speed.

1.2.1 Previously Reported Results of Quantitative Imagery

As presented in the previous report,⁵ the initial analysis of the imagery data focused on determining parameters that were directly comparable to REEDM version 7.07 predictions using default input parameters (i.e., tabulated in that report). For quantitative imagery, the most accurately determined quantities are the cloud's rise time, its stabilization height, the cloud's speed, and its ground track. For Titan IV #K16, T-0.7 h REEDM predictions were substantially different from those measured by imagery. According to the quantitative visible imagery from UCS-7 and Press sites, the cloud took 3.5 min to stabilize (20% faster than predicted), stabilized at 1023 m in altitude (35% higher than predicted), moved in a south-southwesterly direction (versus the east-southeasterly prediction), and moved at an average speed of 3.6 m/s (38% slower than predicted).

1.2.2 Previously Reported Results of Aircraft HCl Measurements

The aircraft's Geomet total HCl detector sampled the ground cloud and possibly the launch column from the Titan IV #K16 launch and recorded HCl concentration data as a function of time and aircraft position. At early times (3–20 min) and at late times (> 76 min), the aircraft encounters fell along a southerly trajectory that was consistent with the imagery-derived ground cloud track and with REEDM's prediction for the rising ground cloud. At intermediate times, the aircraft encounters concentrated on higher altitudes in the southeast quadrant. Although most of the aircraft's HCl measurements were at altitudes within the imager-derived vertical extent of the stabilized ground cloud, the aircraft concentrated mainly on the higher altitude portion of the ground cloud (and possibly the launch column) that moved out to sea. The imagery documented that the lower portion of the ground cloud continued to move to the southwest of the pad. Likewise, the aircraft detected low-altitude pockets of HCl to the south of SLC-41 during its return to the runway. One should remember three things when comparing the aircraft and imagery data: (1) the aircraft's GPS altitude could be off by ± 250 m, (2) the aircraft sampled for longer times than available by imagery, and (3) the aircraft did not probe the full extent of the ground cloud.

The purpose of the earlier report⁵ was to document the quality and quantity of the aircraft data available for validating dispersion models. The aircraft's Geomet data (i.e., total HCl concentration

measurements) were reported in several graphical formats (Chapter 3⁵) to facilitate comparison with REEDM predictions (Appendix A⁵), meteorological data (Appendix B⁵), and imagery data (Chapter 2⁵). The aircraft setup was described in Appendix C.⁵ However, it would be difficult to extract the data for a single pass through the cloud from the summary plots that contain 36 passes through the cloud. Therefore, this report provides the data in a more detailed graphical form that should allow direct comparison to model predictions.

The Geomet detector appears to be useful for aircraft sampling of launch clouds. Several previous reports¹³⁻¹⁵ provided data that illustrated quantitative integrated response as well as excellent temporal and spatial accuracy for mapping the extent and position of Titan IV clouds. Data⁴ also documented significant differences in the HCl concentrations reported by the Geomet and another detector that flew on the #K15 mission. It was illustrated that the concentration reported by both detectors is a strong function of their response functions (i.e., averaging time).

It was suggested that the Geomet reports an HCl concentration that represents an average value for at least an 18-s averaging time.⁴ In contrast, the temporal and spatial accuracy of the Geomet is consistent with an averaging time of only 3 to 4 s.⁴ Therefore, we recommend the use of caution when comparing measured HCl concentration to predicted HCl concentration since the averaging times associated with the detector are not the same as those used in typical dispersion model runs. Certainly, the Geomet's values must be lower than the actual HCl concentrations since it has a finite response time. However, the pre- and post-flight calibrations document quantitative integrated response as deployed for the #K16 mission.

1.2.3 Additional Analysis Included in This Report

This report extends the analysis of the #K16 ground cloud measurements by comparing the results of the aircraft's HCl measurements to the imagery-derived extent of the exhaust cloud. This comparison correlates the aircraft's HCl measurements with the imagery for the first 6 min after launch to document the dimensions and concentration distributions within the rising and the stabilized ground cloud. A similar comparison was reported previously for the #K23 and #K15 ground cloud measurements.^{13,14} This report also documents the aircraft's measurements of the #K16 ground cloud's HCl concentrations to greater spatial and temporal resolution than covered in the test overview.⁵ The detailed graphical analysis of the aircraft's HCl concentrations includes profiles using time and Cartesian coordinates for each 10-min time window for the first 88 min after launch. In addition to cloud concentrations, one can extract angular spreads and cloud dimensions for favorable transects. The results of this graphical analysis are summarized in a table within this report. A similar graphical treatment was reported previously for the #K15 and #K23 ground cloud measurements.^{14,15}

These detailed analyses provide the data in a format that allows direct comparison to model runs for specific times, altitudes, and distances from the release site. The aircraft and imagery results are also available as comma-separated-variable files providing time, latitude, longitude, altitude, Geomet response, HCl concentration, and imagery-derived extent of the ground cloud. The intent of the MVP is to document the results in sufficient detail to validate dispersion models. This report is available electronically as a PDF file that can be viewed in color using ACROBAT[®] viewer (free over the Internet).

2. Analysis

The Volume 1 report⁵ provided a test overview and data summary. That earlier report also provided a detailed description of the analysis methods used both for the imagery and for the aircraft's HCI measurements. Therefore, it is only necessary to provide the reader a brief review in this report.

2.1 Linear Interpretation of Imagery

There are several approaches to analyzing imagery. The simplest approach is to assume that the X pixels (i.e., horizontal pixels) correspond to azimuth and the Y pixels (i.e., vertical pixels) correspond to elevation. This is an excellent assumption for an image recorded with the camera held horizontal or with a camera only slightly inclined while using a reasonably narrow field of view. The equations used in the linear interpretation of the imagery are:

$$dX \times \text{hdpp} = dAZ \quad \text{where hdpp} = \text{horizontal degrees per X pixel}$$

$$dY \times \text{vdpp} = dEL \quad \text{where vdpp} = \text{vertical degrees per Y pixel}$$

Using known landmarks, one can calculate the azimuth (AZ) and elevation (EL) from the imagery site to each landmark. Therefore, the "X,Y" pixel pair that corresponds to each known landmark is calibrated in terms of AZ and EL from the imagery site. If one has two landmarks in an image, one can calculate the dX and dY (i.e., number of pixels) that correspond to the dAZ and dEL (i.e., number of degrees) between the landmarks. Therefore, one can calculate the hdpp and vdpp (i.e., number of degrees per pixel) for the horizontal and vertical axes, respectively. Knowing the total number of horizontal (640) and vertical (480) pixels in the image, one can calculate the horizontal and vertical field-of-view (FOV) of the image. Lastly, for any image that is calibrated (i.e., known landmark and known FOV), one can calculate the AZ and EL for any other pixel in the image using the "linear" correlation between dX and dY with dAZ and dEL, respectively.

The EL can then be used to calculate the height for an object at a known distance from the imagery site. Likewise, the angular size of an object (i.e., horizontal diameter in degrees azimuth and vertical diameter in degrees elevation) can be converted to physical dimensions if one knows the distance of the object from the imagery site.

Alternatively, when one sees the same object from two sites at the same time, one can calculate the closest approach (i.e., intersection) of the rays defined by the AZ and the EL of the object in the images at each site. The closest approach of such rays triangulates the altitude, latitude, and longitude of the object or feature. We have used this approach to triangulate the Titan IV ground cloud's position and extent by sequential analysis of pairs of imagery from multiple sites.

We recently documented¹⁶ that the linear interpretation of imagery (used in this report) is accurate for low elevations (i.e., less than 20°) and for objects contained within reasonable fields of view (i.e., 20° to 30°). This was the case for the #K16 exhaust cloud imagery.

2.2 PLMTRACK Analysis of Imagery from Two Sites

Brian P. Kasper created and maintains the PLMTRACK program at The Aerospace Corporation. PLMTRACK provides a convenient way of triangulating the position of an object using imagery from two sites. PLMTRACK provided an absolute method of triangulating the position of the abort (or exhaust) cloud without making any assumptions regarding the position of the cloud. The analyst drew a box about the cloud in simultaneously acquired images from two sites. The edges of the box touch the top, left, right, and bottom extremes of the cloud as illustrated by Figure 1 (i.e., the shaded rectangle represents the image boundaries, while the ellipse represents an abort or exhaust cloud). PLMTRACK calculates the nearest approach for various rays, as illustrated by Figure 1 (i.e., as a ground projection of the cloud along with several rays from each camera site). The rays are defined by the middle of each of the edges of the boxes and the center of the boxes. These rays define the broadest extent and the position of the cloud in all observable dimensions as illustrated by the Cartesian plot of PLMTRACK results in Figure 2. In Figure 2, the site locations and rays are actual #K16 ground cloud data, while the outline of the cloud was synthesized for heuristic purposes.

The PLMTRACK analysis documented not only the Cartesian extent of the cloud, as illustrated in Figure 2, but also the x,y,z coordinates for the top, middle, and bottom of the cloud for each pair of images. Therefore, we will compare the imagery-derived maximum extent of the cloud to the extent derived by aircraft HCl sampling of the same exhaust cloud.

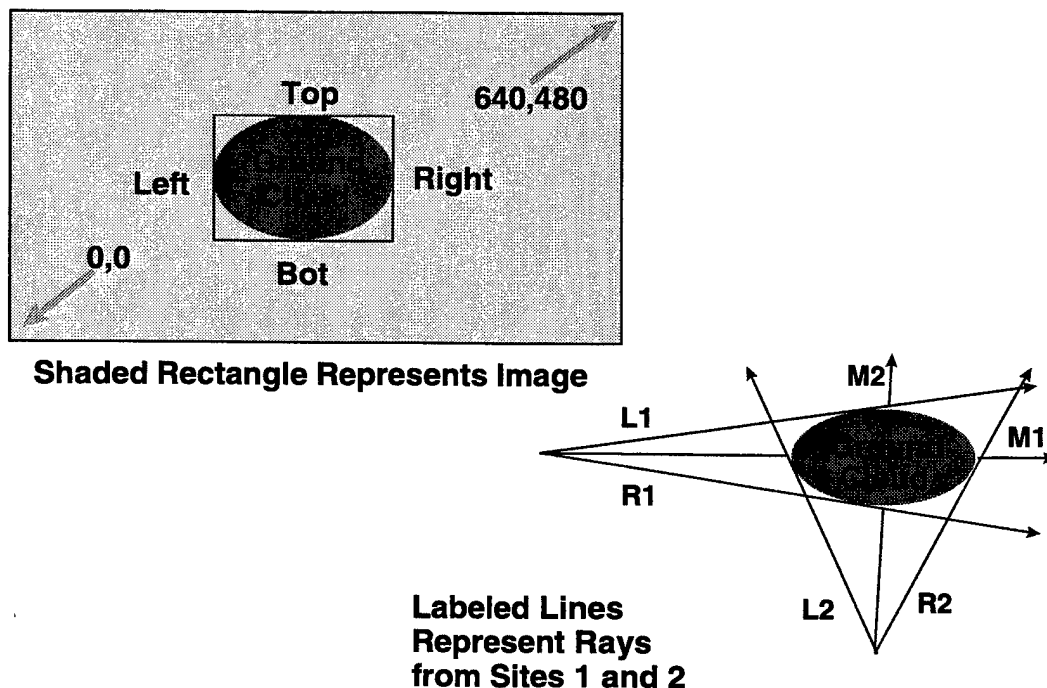


Figure 1. PLMTRACK box method within an image and projected onto ground plane.

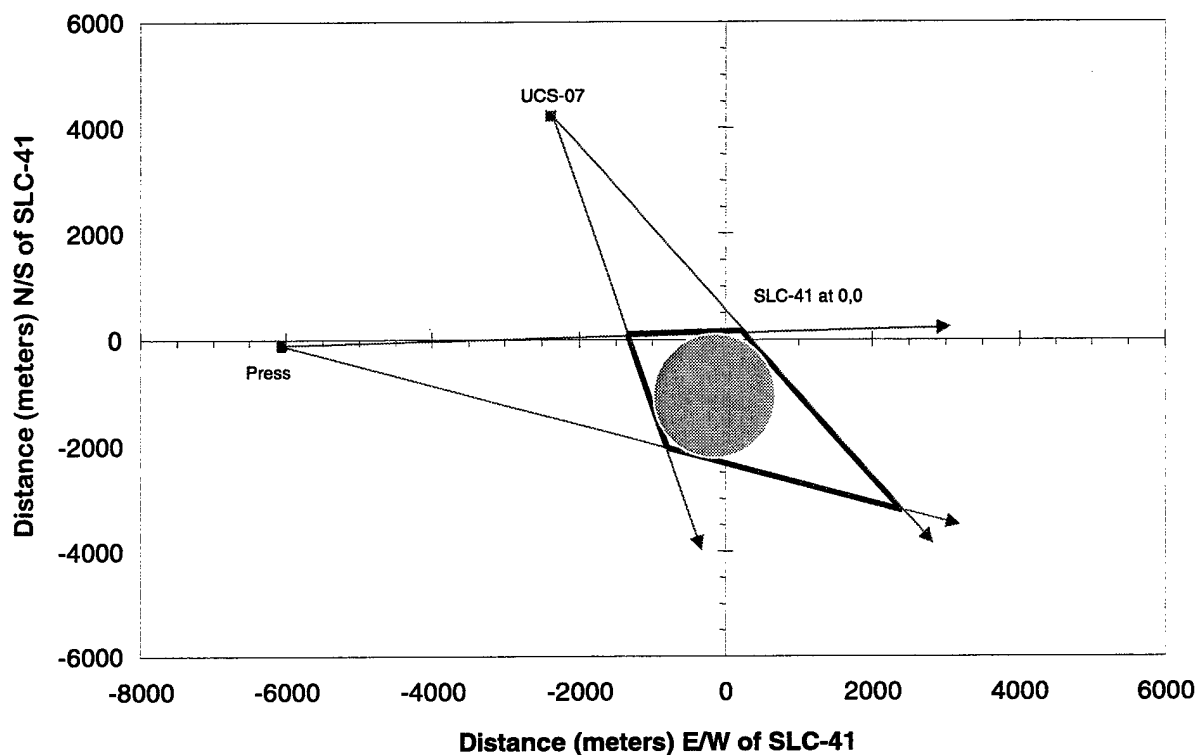


Figure 2. PLMTRACK ray tracing and extent of #K16 exhaust cloud (T+ 4.0 min).

2.3 Geomet HCl Measurements

As described in detail in Chapter 3 of the test overview report,⁵ I-NET, a NASA contractor, modified a Geomet for mounting in the nose of a Piper (PA-44-180) Seminole (a twin-engine, four-seat aircraft). The Geomet is a total HCl monitor that produces a response proportional to the combined HCl present in both the vapor and the aerosol phases. It reports the HCl concentration as parts-per-million (ppm) by volume (i.e., $V_{\text{HCl}} 10^6 / V_{\text{total}}$). This instrument sampled the air through a horizontal 4-ft-long ceramic inlet wetted with a bromate/bromide-containing reagent. The HCl diffuses to the wetted walls of the ceramic tube and produces bromine vapor through reactions with the reagent. The bromine vapor is swept into a buffered hydrogen peroxide/Luminol solution, resulting in photoluminescence detected by a filtered photometric detector. I-NET disabled the Geomet's autoranging electronics so that a single range produced a millivolt response that was proportional to the combined HCl vapor and aerosol concentration entering the inlet. I-NET calibrated the Geomet against HCl vapor before and after the #K16 mission.

SRS Technologies Inc., a contractor, provided an interface between the I-NET laboratory and the Florida Institute of Technology (FIT) flight crew. NASA, NOAA/Air Resources Laboratory/Field Research Division, I-NET, SRS, and FIT cooperated in the integration of the NOAA data system, the FIT aircraft, and the Air Force Geomet into an airborne sampling and data logging system. FIT personnel piloted the aircraft during the #K16 mission, while 45th AMDS/SGPB personnel operated the NOAA data system and the Geomet detector. The NOAA data system logged GPS time and position as well as Geomet response every 0.25 s during the flight. NOAA provided a comma-separated-variable (csv) data file to The Aerospace Corporation.

As stated previously, the aircraft's altitude was measured using a global positioning system (GPS) receiver using regular service (no differential corrections were available for the CCAFS area during this mission). The GPS altitude data were recorded as meters relative to mean sea level (MSL).

2.3.1 Reference for Altitudes

When comparing the aircraft's GPS-derived altitude (i.e., m MSL) to the imagery, rawinsonde, and REEDM data, it is essential to use the same frame of reference for measuring the height. REEDM reports the predicted height of the exhaust cloud relative to MSL as well as above ground level (AGL). In the plots in this report, altitude is relative to MSL.

2.3.2 Geomet Calibration Data

The Geomet's configuration was equivalent for the #K23, #K15, #K22, and #K16 missions. The calibration response curves for the #K16 mission were included in the test overview report.⁵ The Geomet calibrations are HCl vapor challenges using constant concentration for long exposure times. Those data illustrated that the Geomet has an almost instantaneous response to sudden large changes in HCl vapor concentration but requires a longer time to reach the plateau response. Therefore, the Geomet should accurately map the extent, but not necessarily the strength of the Titan IV exhaust cloud.

2.3.3 Geomet Response Characteristics

The response characteristics of the Geomet detector are not perfectly matched to aircraft sampling. As configured for Titan IV missions (#K23, #K15, #K16, and #K22) and as illustrated by the #K16 data included in previous reports,^{4,5} the Geomet requires more than 15 s to reach 90% of its plateau response as deployed for the Titan IV missions. In addition, the response time changes as a result of exposure to HCl vapor (i.e., the second exposures were faster than the first exposures after coating the inlet). This is consistent with passivation of active sites within the freshly coated inlet. The magnitude of plateau response, as well as the time to reach it, can worsen when the exposure times are extremely long (as in the #K16 mission, which had an hour hold prior to extended sampling of the launch cloud). This is consistent with depletion of the reagent that coats the inlet. For all of the Titan IV missions, the Geomet's inlet was coated with reagent once prior to the flight. Therefore, one would expect some variation in response characteristics during each sampling mission. In spite of these difficulties, we believe the Geomet has some useful features that are discussed in the following paragraphs.

2.3.3.1 Accurate Integrated HCl Dose

The Geomet's raw response and its integrated response were plotted against time for the mission #K16 pre-flight and post-flight calibrations in previous reports.^{4,5} Those plots documented that the Geomet accurately integrated the total HCl dose for HCl vapor exposures. There was quantitative behavior (i.e., more than 98% of total dose) for the pre-flight calibration and over 92% of total dose for the post-flight calibrations. Since the Geomet was configured similarly for all of the Titan IV missions, the #K16 response data provide an interesting complement to the less detailed calibration data available for other missions.⁴ Since the Geomet provides accurate total HCl dose for each pass

through the cloud, one can calculate the average HCl concentration using the time of the exposure and the total dose. The following paragraphs discuss cloud edge detection by the Geomet. Accurate edge detection is the same as accurate exposure time measurement.

2.3.3.2 Accurate Edge Detection and Peak Location Reporting

Since the aircraft is moving at more than 70 m/s, and it takes 15 s (or more) for the Geomet to provide 90% response to the new HCl concentration, it is likely that the Geomet may underestimate the maximum HCl concentration for short encounters with the cloud. However, the initial response to 10% of the plateau response is extremely rapid. Thus, there should be little offset between the Geomet's first indication of change and the aircraft's encounter with the edge of the exhaust cloud or the maximum concentration within the exhaust cloud. This was demonstrated in previous reports.

The temporal, relative, and absolute accuracy of the Geomet's response to the Titan IV #K15 exhaust cloud was documented for the first few minutes after launch by comparison of the Geomet's cloud data to that of the Spectral Sciences gas filter correlation (GFC) spectrometer that flew on the same aircraft for the #K15 mission. The GFC spectrometer provided an instantaneous response to the exhaust cloud and was mounted beneath the aircraft. The inlet to the Geomet extended out of the front of the same aircraft.

The data from the GFC data were compared⁴ to the Geomet data to establish the significance of the Geomet's response characteristics for actual aircraft sampling of Titan IV #K15 exhaust cloud. The HCl concentration profile was derived in three ways for a single cloud pass: (1) Geomet response, (2) 3.85 s averaging of the GFC data, and (3) 18 s averaging of the GFC data. Careful comparison of these data revealed no shift in time between the maximum concentration reported by the 3.85 s GFC spectrometer data and the maximum reported by the Geomet detector. A 6–12 s shift in time would have corresponded to a 0.5–1 km shift in position for the maximum of the cloud based upon a 70 m/s aircraft speed. The width (i.e., onset of rise and start of fall) is identical for the Geomet and for the 3.85 s GFC spectrometer data. This is consistent with good edge detection by both detectors. Comparison of the 18-s GFC data to the Geomet data documented the same value for the maximum HCl concentration but not the same temporal (i.e., positional) mapping of the cloud. Therefore, those data were consistent with the Geomet's documented two-part response curve: (1) rapid initial response to a large change in HCl concentration and (2) a slow rollover in response prior to reaching a plateau. Since the Geomet has both fast and slow components of response, it appears that the Geomet is able to accurately map the extent and shape of the exhaust cloud by virtue of its fast response to large changes in concentration. The tail on the Geomet peaks was consistent with the tail (i.e., slow recovery to baseline) observed during challenges against calibration vapors.

Since the GFC technique only responds to vapor while the Geomet responds to total HCl (aerosol and vapor), this treatment cannot provide quantitative rise characteristics for the Geomet. In addition, the noisy GFC data may overestimate the integrated HCl (i.e., bigger area than Geomet). However, one can conclude, qualitatively, that the Geomet not only provides integrated HCl for each pass through the cloud but also maps the extent and position of the cloud by virtue of the fast component of its complicated response function. Therefore, one can calculate the average HCl concentration for each pass through the cloud from the accurate extent (i.e., time in the cloud) and the accurate total HCl dose (i.e., ppm-s).

3. Results

The results of the quantitative analysis of the ground cloud imagery were documented in a previous report⁵ as were the results from the Geomet sampling of the HCl within the ground cloud. This report extends the analyses in two ways: (1) correlation between the aircraft Geomet's HCl concentration profiles and the imagery-derived maximum extent of the ground cloud and (2) graphical reporting of the aircraft Geomet's HCl data with greater spatial and temporal resolution than was possible in the data summary report. Simultaneous imagery and aircraft sampling data are available for the first 6 min after launch and are compared in the first portion of the results. The second portion of the results discusses the standardized series of plots that are included in Appendix B and cover each 10-min period. The third portion of the results summarizes the entire 88 min of aircraft sampling data. This method of reporting the aircraft's HCl results allows direct graphical comparison with dispersion model output.

3.1 Comparison of Aircraft HCl Profiles to Imaged Ground Cloud Extent

The first three aircraft encounters with the exhaust cloud (i.e., passes through the cloud) occurred between 3 and 7.4 min after launch. During this same period, the quantitative visible imagery documented the full extent of the exhaust cloud. This section provides Cartesian plots that overlap the aircraft's HCl sampling data with the imagery-derived extent of the exhaust cloud. These data illustrate consistent edge detection by the aircraft and by the quantitative imagery. In addition, a second series of plots document the instantaneous HCl concentrations, the average HCl concentrations, and the time in the exhaust cloud for each of the first nine aircraft encounters with the exhaust cloud. For completeness, this section also provides an altitude plot for the imagery-derived extent of the cloud and for the aircraft Geomet's HCl concentration data. Therefore, this section provides an imagery-derived three-dimensional extent for the ground cloud as well as aircraft-derived (i.e., Geomet) HCl concentration profiles within well-identified regions of the ground cloud.

3.1.1 Cartesian Extent of the Ground Cloud for Passes 1-3

Figure 3 documents aircraft-derived and imagery-derived exhaust cloud data collected between 3 and 7.4 min after launch. In Figure 3, the aircraft's Cartesian trajectory is plotted with different symbols to indicate the measured HCl concentrations at each point. For comparison, Figure 3 also includes selected imagery-derived polygons that document the maximum extent of the exhaust cloud over a similar period. Figure 3 reveals that the extent of the exhaust cloud is mapped identically both by the aircraft's Geomet HCl monitor and by the quantitative imagery. Likewise, both methods document movement of the cloud in a southerly direction between 3 and 7.4 min after launch.

Figures 4 through 6 document individual Cartesian plots for each of the three passes shown in Figure 3. The arrows indicate the direction of travel and, therefore, the later data are closer to the head of the arrow than the earlier data. In each case, the leading edge (i.e., earliest HCl hits) reported by the

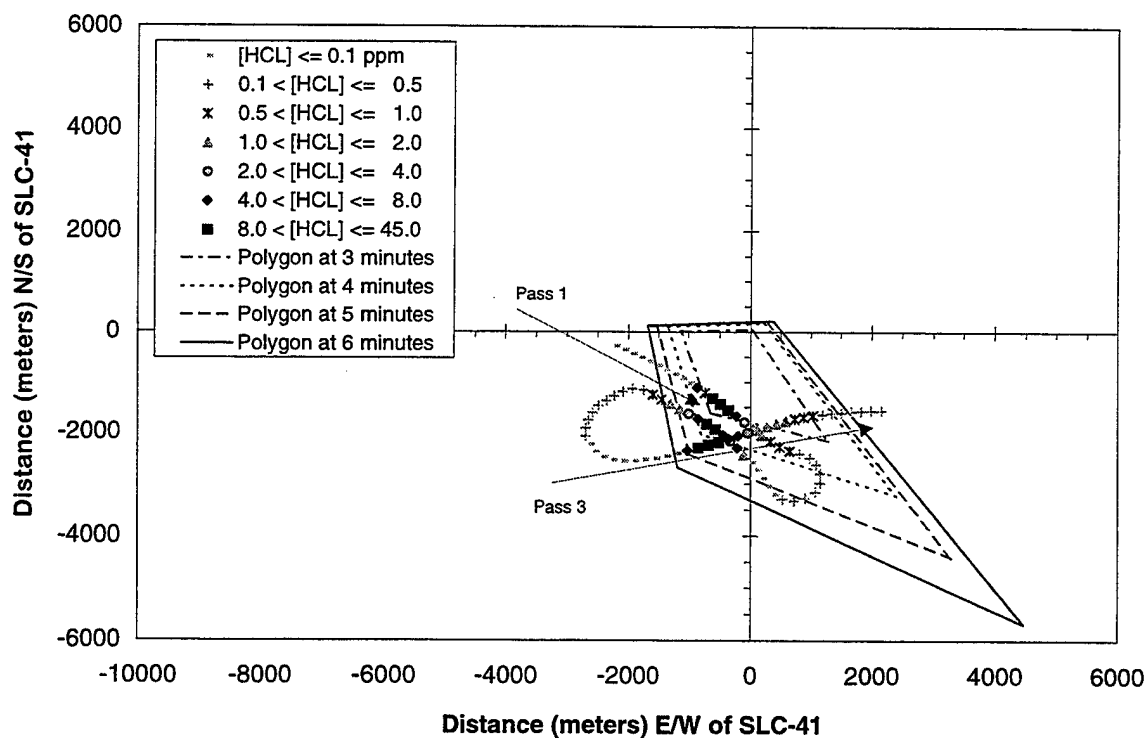


Figure 3. Imagery- and aircraft-derived Cartesian extent for #K16 cloud (T=3-7.4 min).

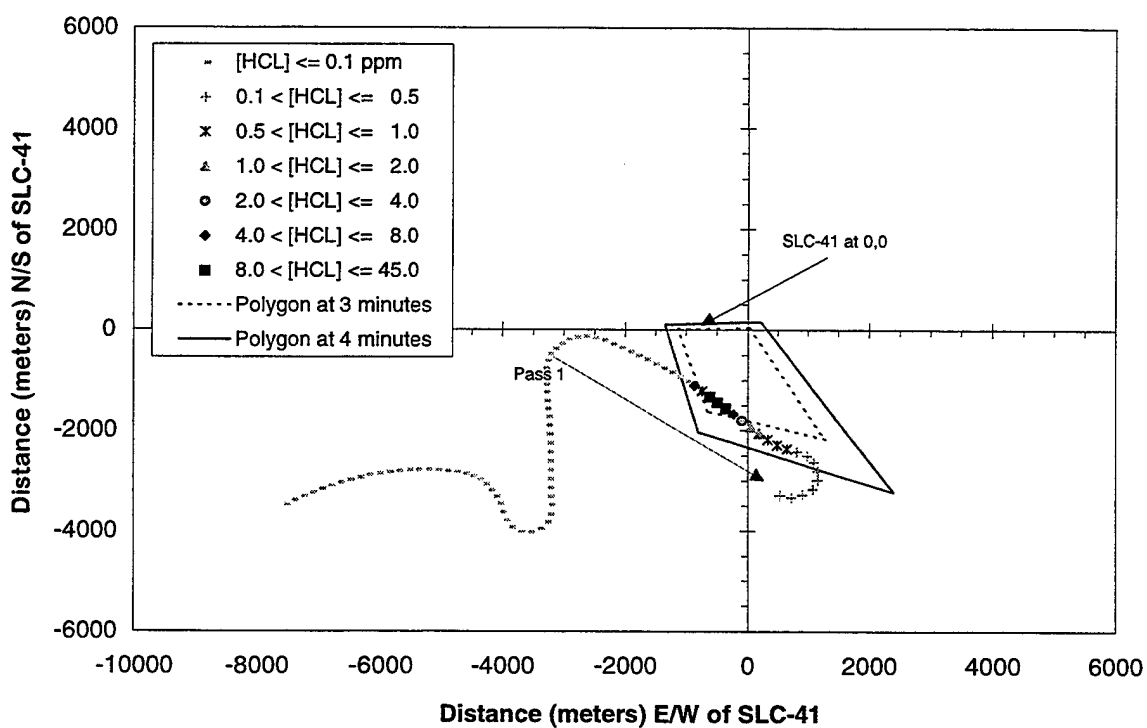


Figure 4. Aircraft pass 1 (T=0-4.5 min) versus imagery-derived polygons (T=3-4 min).

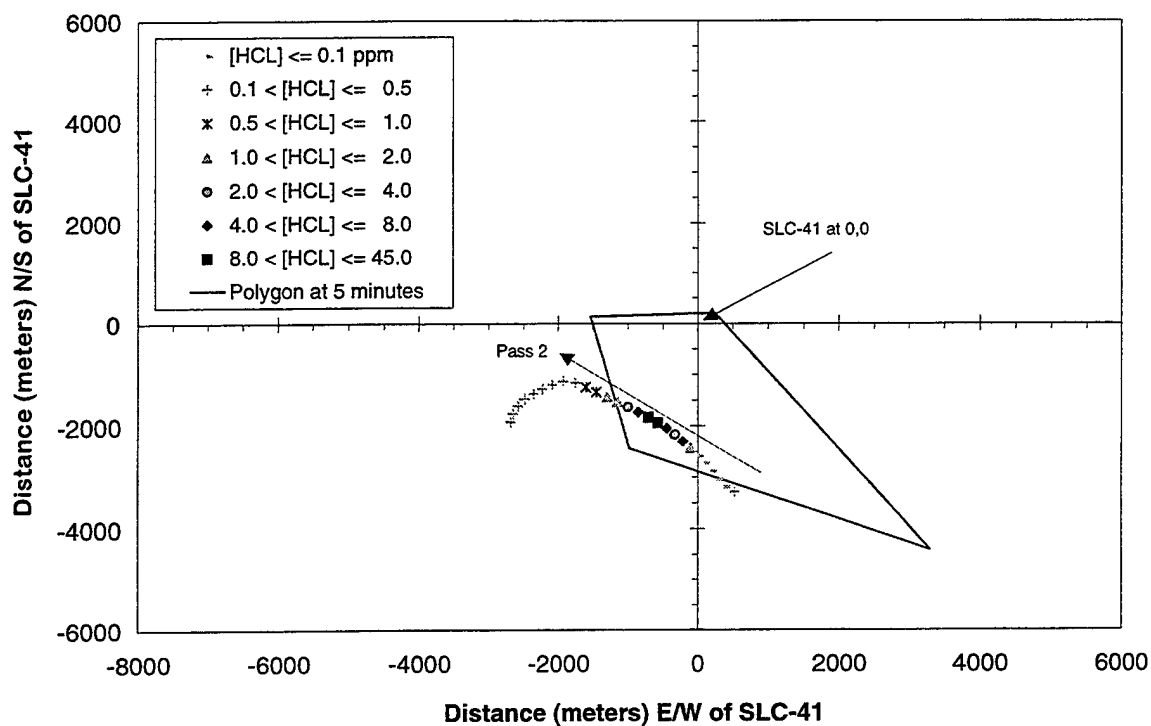


Figure 5. Aircraft pass 2 (T=4.5-5.8 min) versus imagery-derived polygon (T=5 min).

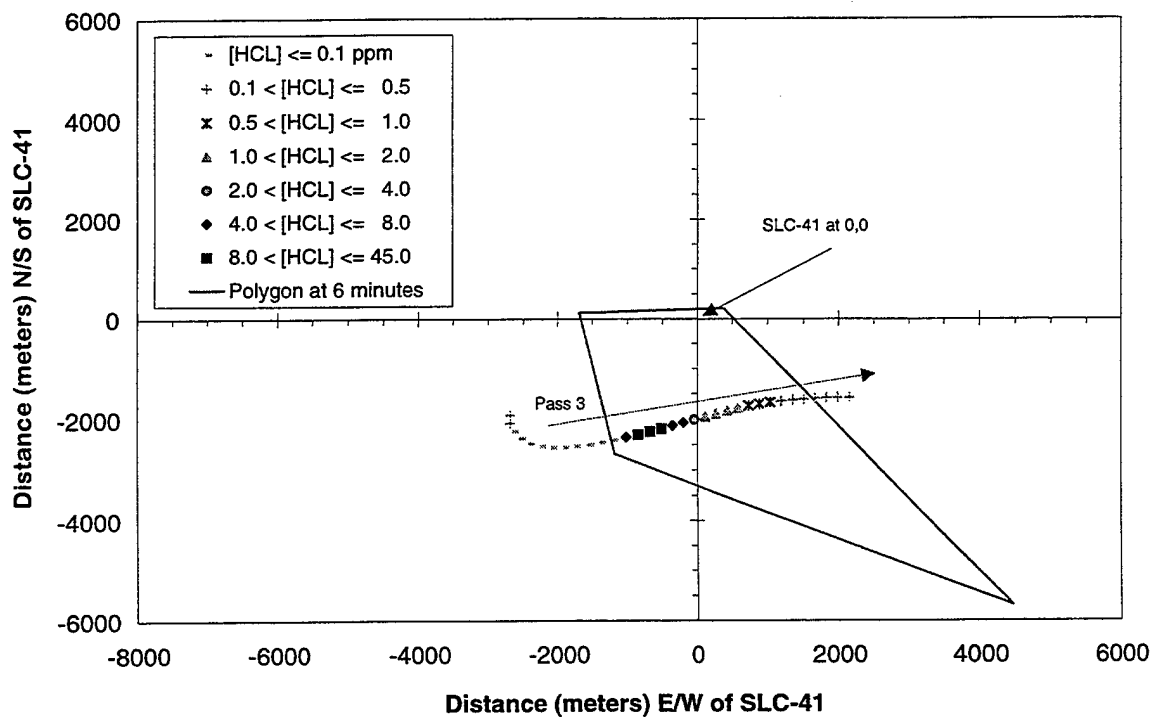


Figure 6. Aircraft pass 3 (T=5.8-7.4 min) versus imagery-derived polygon (T=6 min).

aircraft's Geomet detector are consistent with the edge of the imagery-derived maximum extent (i.e., polygon) of the exhaust cloud. To be consistent with the imagery, the Geomet should not report significant HCl concentration outside of the imagery-derived polygon. As documented in the prior #K15 report,⁴ the Geomet detector provides a fast initial indication of exposure but is slow to recover (i.e., has a long tail in its recovery curve). Therefore, it is expected that the aircraft will continue to report decreasing HCl concentrations after it has already exited the exhaust cloud. Review of Figures 4 through 6 confirms that the slow recovery produces decreasing HCl concentrations (i.e., an artifact) that extend beyond the imagery-derived polygon only on the tailing leg (i.e., later hits) of each aircraft encounter with the exhaust cloud. However, in spite of this long tail, the aircraft's HCl measurements do map the tailing edge of the exhaust cloud as the last high-level hit preceding the Geomet's slow recovery (i.e., decreasing HCl concentrations after the encounter). Review of Figures 4 through 6 reveals a fairly consistent detection of the tailing edge of the exhaust cloud by using the last strong HCl hit (i.e., HCl > 2 ppm for passes 1 through 3) from the aircraft and the edge of the imagery-derived polygon. One must remember that the polygon represents the maximum observable extent (i.e., the analyst's choice) at all altitudes while the aircraft sampled the cloud at one altitude for each encounter. Therefore, the bulk of the cloud is contained in the imagery-derived polygons, and the aircraft hits should fall within the polygon.

Figures 7 and 8 are visible exhaust cloud images that reveal the extent of the cloud as viewed from UCS-07 and Press sites at T+5.0 min after launch. Based upon review of Figures 7 and 8, the imagery-derived maximum extent of the ground cloud (i.e., for all altitudes) will probably be greater than the extent sampled by any aircraft encounter (i.e., at a single altitude). This is consistent with the fact that the extent mapped by the imagery-derived polygons (i.e., Figures 4–6) was larger than the extent of the highest HCl concentration hits (i.e., extent of the cloud by the Geomet detector) for every aircraft encounter. The complicated cloud structure shown in Figures 7 and 8 is also consistent with the large fluctuations in HCl concentration within the cloud. As shown previously,⁵ and in a later section of this report, the Geomet detector documents large fluctuations in the HCl concentration during each aircraft encounter with the exhaust cloud.

3.1.2 Average HCl Concentration and Total HCl Dosage for Passes 1–9

The analysis section documented two useful properties of the aircraft's Geomet HCl detector: (1) accurate mapping of the edge of the exhaust cloud (and the position of maximum concentration) and (2) quantitative reporting of the total HCl dosage. In the previous section, Figures 3 through 6 supported the claim that the Geomet accurately detects the edge of the cloud. Those plots compared the aircraft's HCl data to the imagery-derived maximum extent of the exhaust cloud. In regards to total HCl dosage, Figures 9 through 17 plot the aircraft's HCl concentration against time for each of the first nine passes through the #K16 exhaust cloud. The horizontal line in these figures documents the average HCl concentration within the cloud as height and the time spent in the cloud as length. Integration of the total area under the response curves (i.e., including the long tail) provides the total HCl dosage (ppm-s) for each encounter. The following analysis includes several corrections and provides error limits for these results.

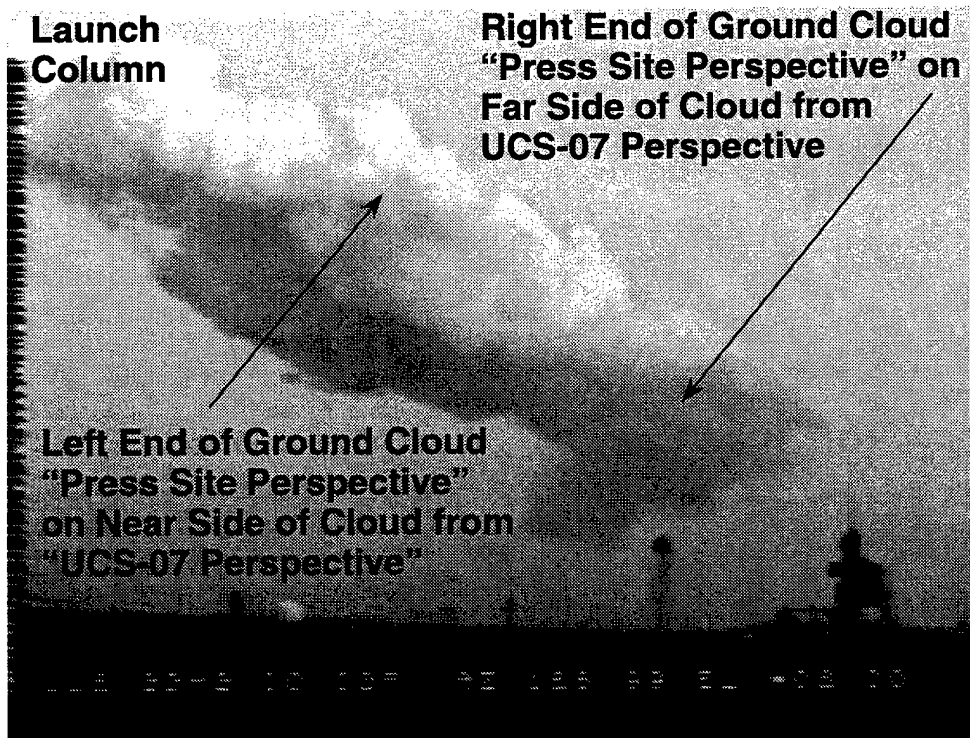


Figure 7. Visible image of ground cloud (T+5.0 min) from UCS-7 site.

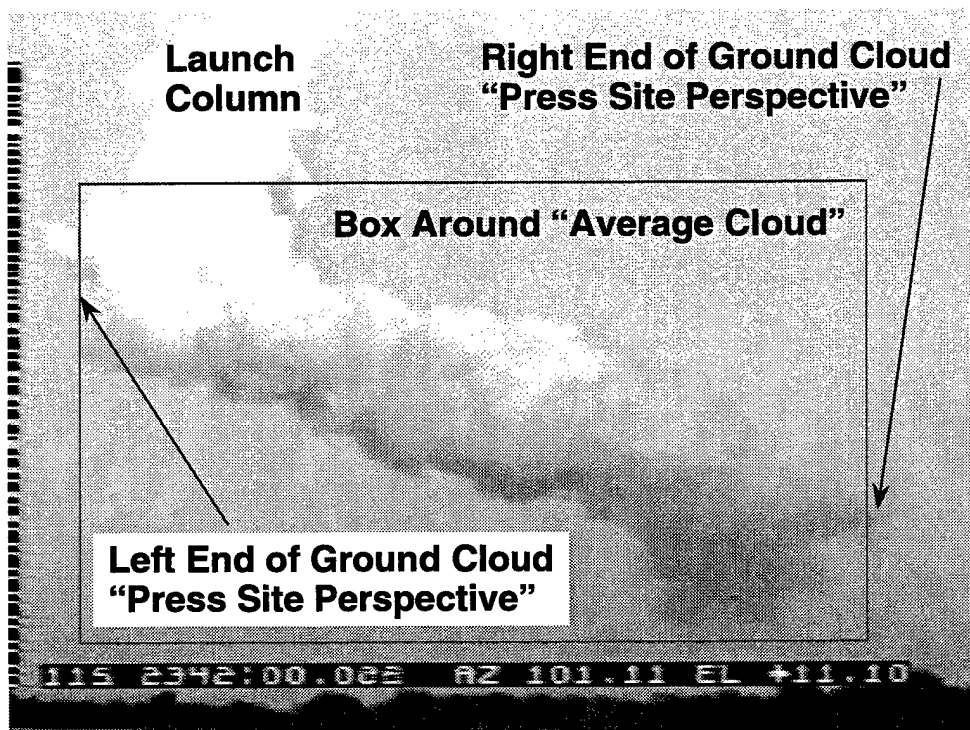


Figure 8. Visible image of the ground cloud (T+5.0 min) from Press site.

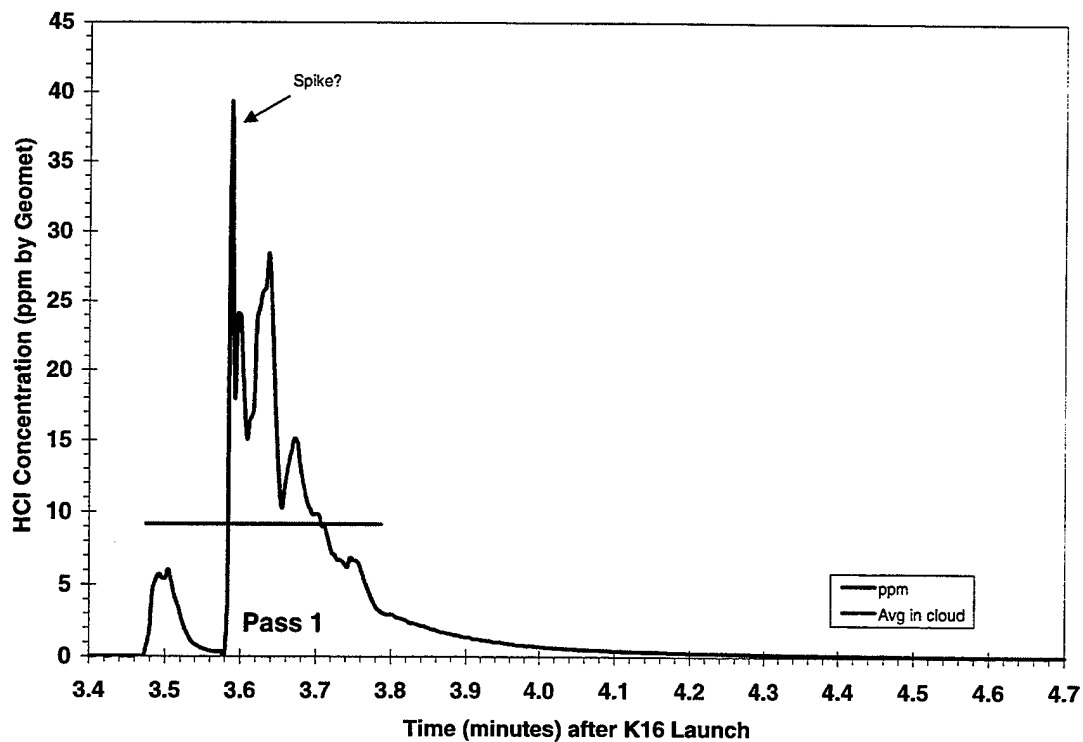


Figure 9. Aircraft pass 1 (T=3.4-4.7 min) HCl concentration and dosage data.

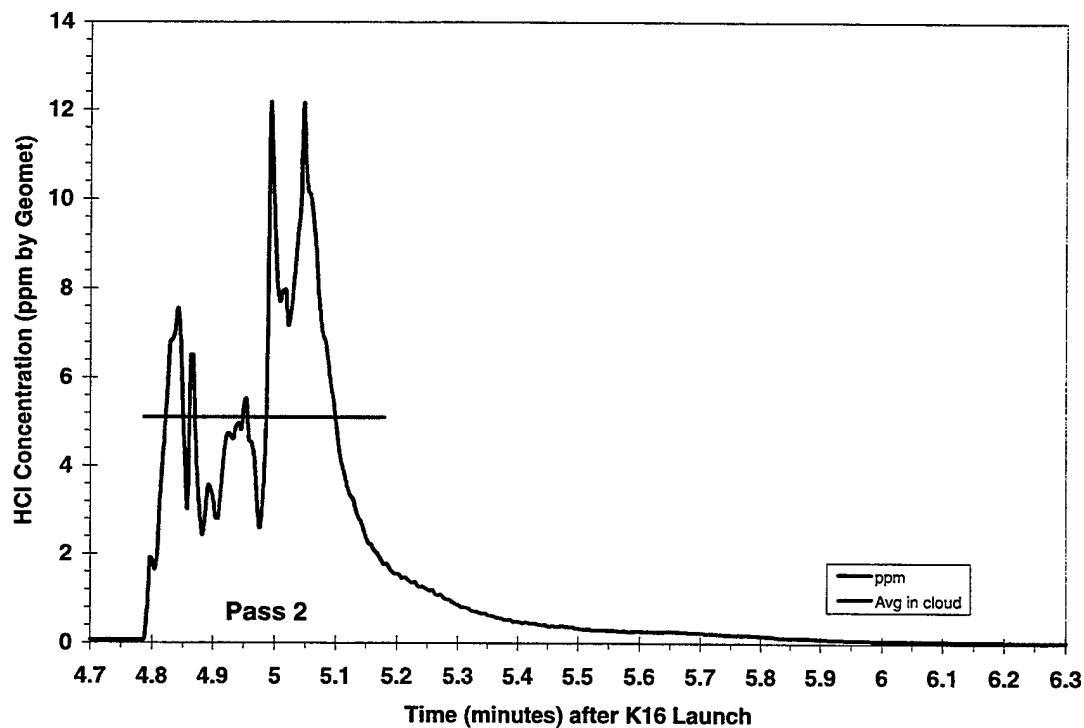


Figure 10. Aircraft pass 2 (T=4.7-6.3 min) HCl concentration and dosage data.

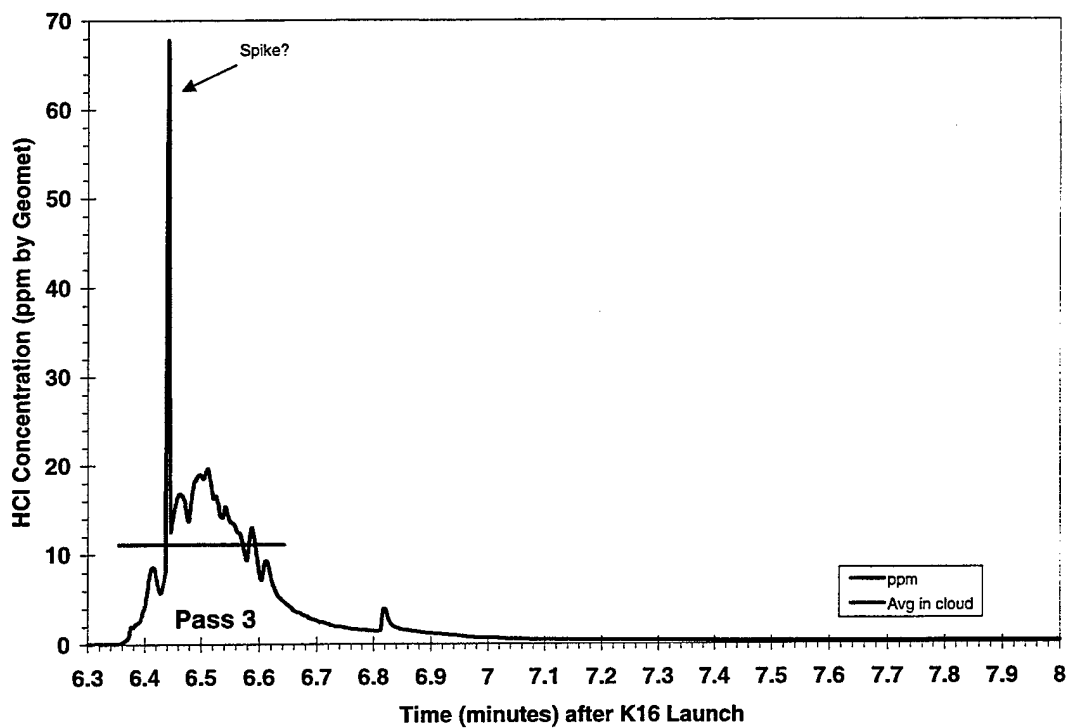


Figure 11. Aircraft pass 3 (T=6.3-8.0 min) HCl concentration and dosage data.

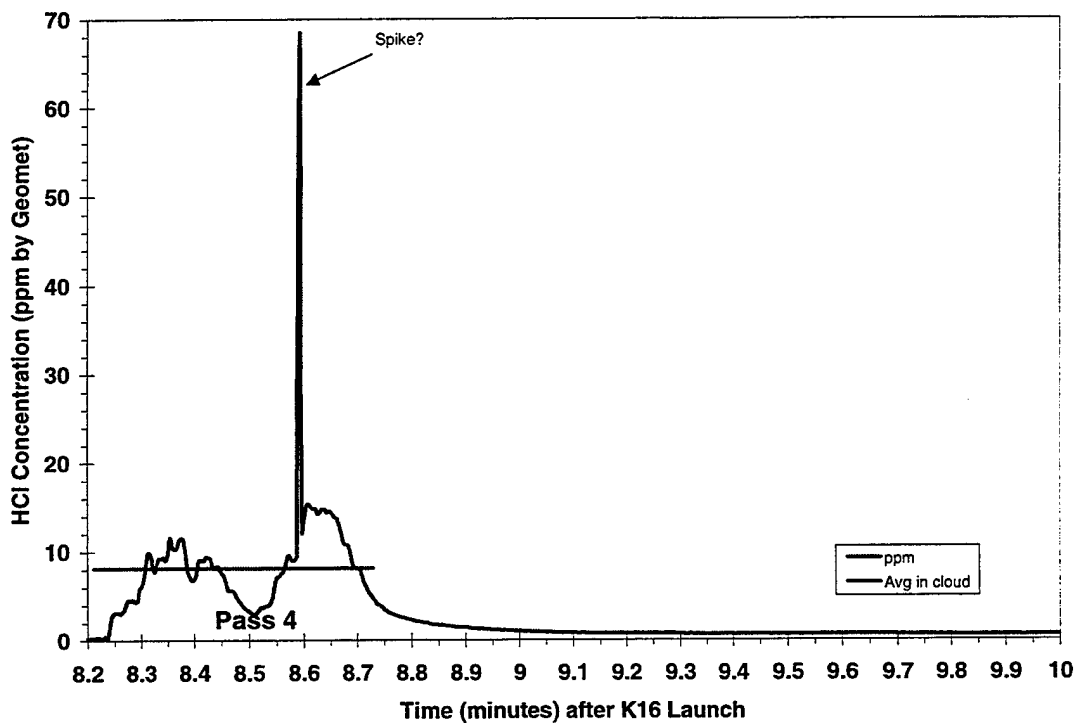


Figure 12. Aircraft pass 4 (T=8.2-10 min) HCl concentration and dosage data.

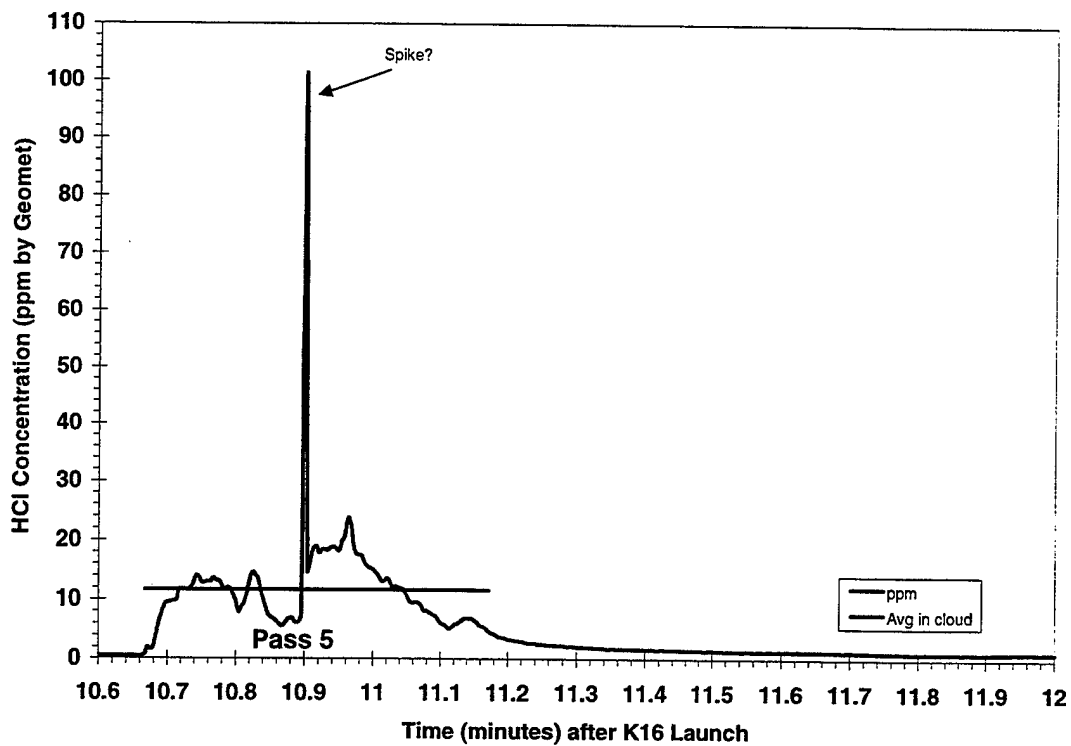


Figure 13. Aircraft pass 5 (T=10.6-12 min) HCl concentration and dosage data.

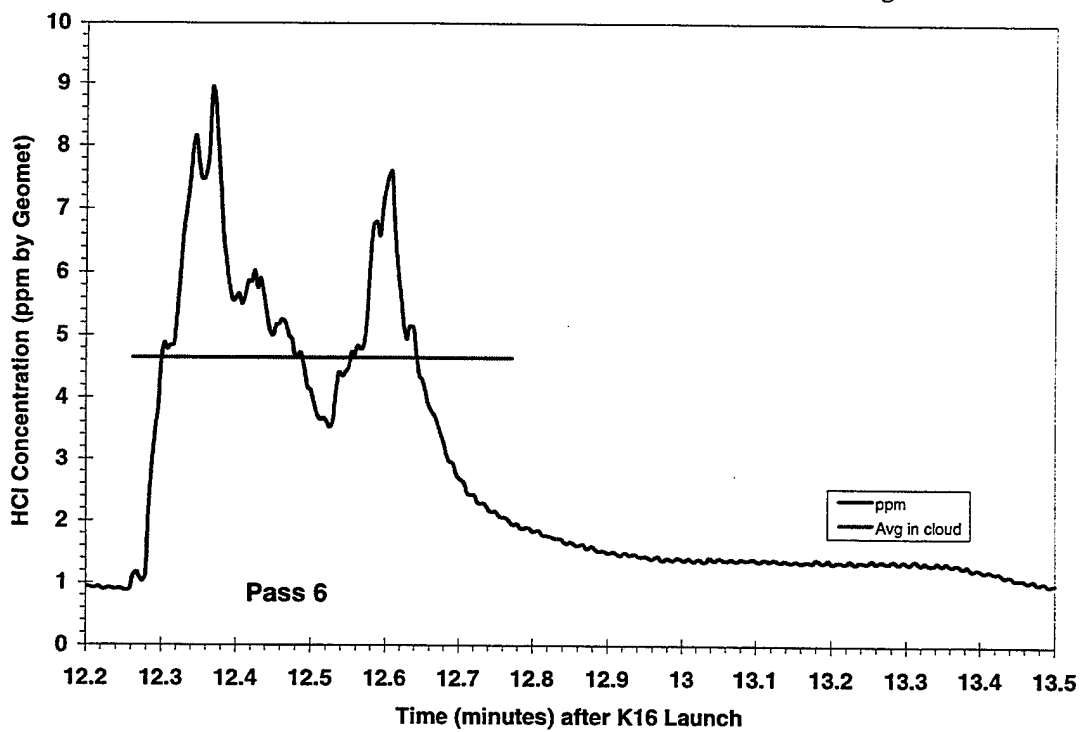


Figure 14. Aircraft pass 6 (T=12.2-13.5 min) HCl concentration and dosage data.

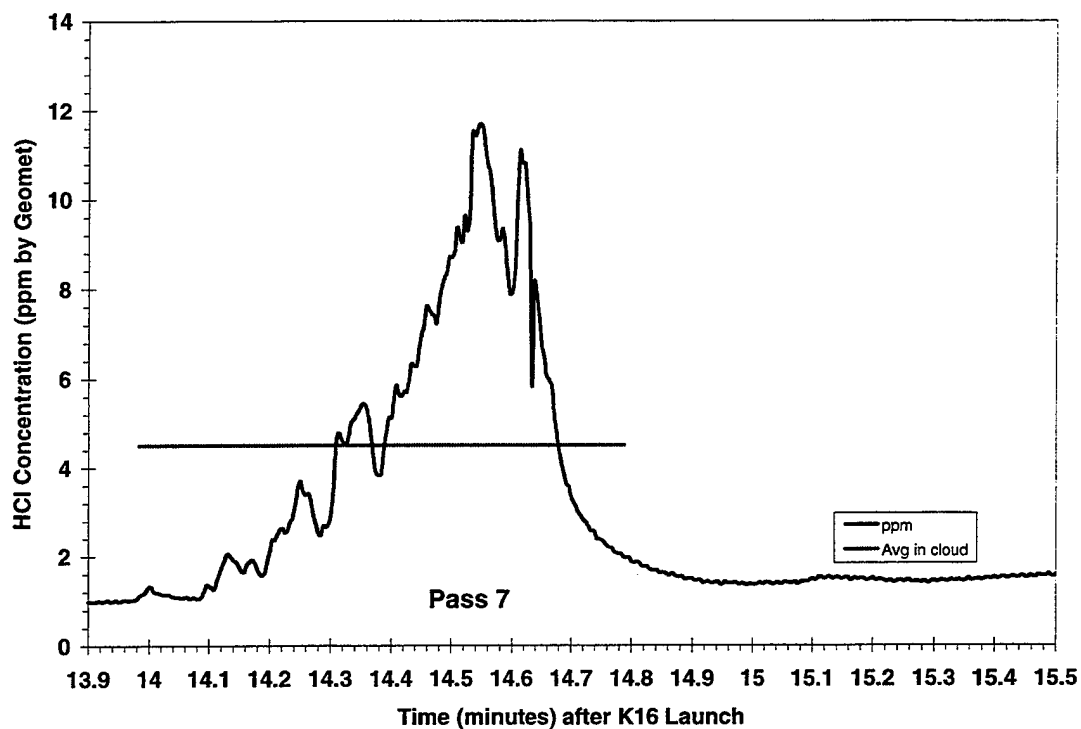


Figure 15. Aircraft pass 7 (T=13.9-15.5 min) HCl concentration and dosage data.

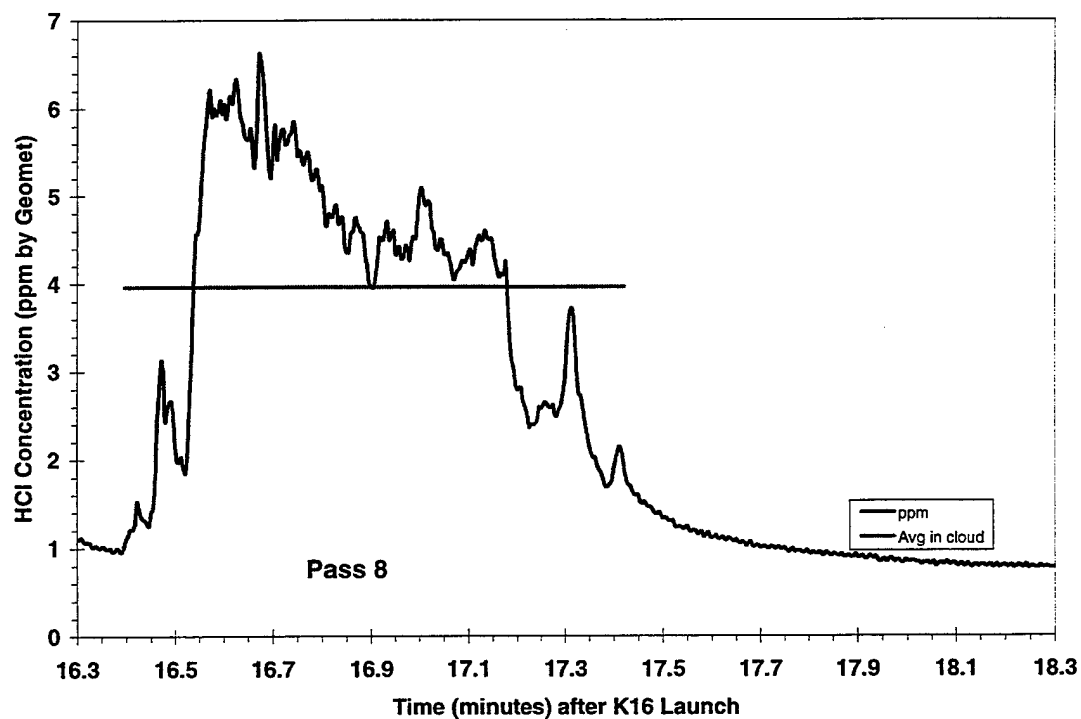


Figure 16. Aircraft pass 8 (T=16.3-18.3 min) HCl concentration and dosage data.

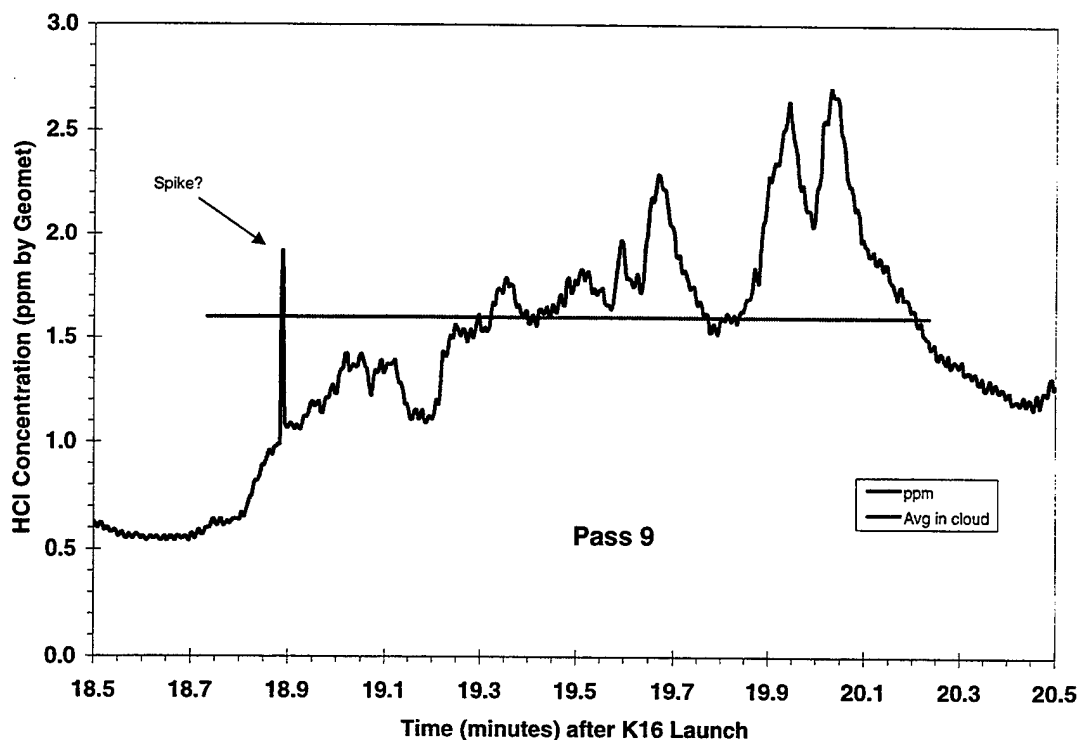


Figure 17. Aircraft pass 9 (T=18.5-20.5 min) HCl concentration and dosage data.

Table 1 summarizes the HCl concentration data for passes 1–9. The first column identifies the pass (i.e., encounter). The next two columns report the time within the cloud (i.e., tc) and the integration time (i.e., ti) used to calculate the total HCl dosage. The next four columns report the average HCl concentration within the cloud. [HCl]c is an average of the HCl concentration while within the cloud (i.e., tc). [HCl]c-b is the difference between [HCl]c and the background HCl concentration (i.e., Bkgd in column 8 of the table). The background is the initial offset in the baseline and includes the asymptotic tail from prior cloud encounters. [HCl]c-s is an average after excluding any HCl spike that occurred within the cloud. The HCl spikes are identified in Figures 9, 11–13, and 17 for passes 1, 3–5, and 9, respectively. These spikes might be electronic glitches due to radio transmissions and

Table 1. Summary of HCl Concentration Data for Passes 1–9

Pass (#)	tc (min)	ti (min)	[HCl]c (ppm)	[HCl]c-b (ppm)	[HCl]c-s (ppm)	[HCl]c-s-b (ppm)	Bkgd (ppm)	f(HCl)c (% total)	f(HCl)c-b (% total)	f(HCl)c-s (% total)	f(HCl)c-b-s (% total)
1	0.312	1.208	9.2	9.2	8.7	8.7	0.0	84	84	85	85
2	0.392	1.513	5.1	5.0	#N/A	#N/A	0.1	83	86	#N/A	#N/A
3	0.288	1.646	11.1	11.1	10.3	10.3	0.0	77	78	78	79
4	0.517	1.784	8.2	7.9	7.7	7.4	0.2	77	81	72	76
5	0.504	1.258	11.6	11.2	10.9	10.4	0.5	83	86	82	86
6	0.509	1.238	4.6	3.7	#N/A	#N/A	0.9	70	83	#N/A	#N/A
7	0.804	1.517	4.5	3.5	#N/A	#N/A	1.0	77	89	#N/A	#N/A
8	1.025	1.904	4.0	3.0	#N/A	#N/A	1.0	82	99	#N/A	#N/A
9	1.500	1.767	1.6	1.0	1.6	1.0	0.6	87	89	87	89

are suspicious because of the large, fast jumps in HCl response. $[\text{HCl}]_{\text{c-s-b}}$ is an average that excludes any spike and subtracts the initial background (i.e., baseline). Immediately following the background (i.e., Bkgd) in the table, there are four fractions that are reported as a percentage of the total dosage. The notation $f(\text{HCl})$ is used to report, as a percentage, the fraction of the total HCl dosage associated with the average HCl within the cloud. For example, a 9.2 ppm average concentration during 0.312 min corresponds to 172 ppm-s, which is 84% of the total 205 ppm-s HCl dosage (i.e., integrated HCl). As with the average HCl, the total HCl dosage was corrected for the baseline, the spike, and for both the baseline and spike. Therefore, $f(\text{HCl})_{\text{c}}$ is based upon uncorrected data. While $f(\text{HCl})_{\text{c-b}}$, $f(\text{HCl})_{\text{c-s}}$, and $f(\text{HCl})_{\text{c-s-b}}$ include corrections for the baseline, the spike, and both, respectively. The corrections are applied both to the average HCl within the cloud and to the total integrated HCl dosage. Total HCl is related to each pair of $[\text{HCl}]$ and $f(\text{HCl})$ entries by the following relationship:

$$(\text{Total HCl dosage}) = [\text{HCl}] \times t_{\text{c}} \times 60 \times 100\% / f(\text{HCl}) = (\text{HCl dosage in cloud}) \times 100\% / f(\text{HCl})$$

It is apparent from a review of Table 1 that the corrections are on the order of a ppm for the average HCl concentration and 10% for the fractional difference between the "in cloud" and "total" HCl dosages. These results suggest reasonably accurate HCl concentrations within the cloud. The average concentration within the cloud accounts for over 70% of the total HCl dosage for every encounter. As mentioned previously, the corrections (i.e., baseline and/or spike) were applied consistently both to the average HCl and to the integrated HCl dosage that were used to calculate the fractional difference.

So far, we have the average concentration within the cloud and the horizontal extent for each of the first three passes through the exhaust cloud. In the next section, we provide the vertical extent and, thereby, complete our 3-D picture of the exhaust cloud.

3.1.3 Aircraft Altitude and Imagery-Derived Vertical Extent for Passes 1-4

The previous sections documented the Cartesian extent, the average concentration, the total HCl dose, and the time spent in the exhaust cloud for each of the first nine aircraft encounters with the exhaust cloud. For the first three encounters, comparison of the aircraft's Cartesian extent with the imagery-derived maximum extent revealed that the aircraft flew through the most southerly end of the imagery-derived horizontal extent of the ground cloud. Figure 18 documents the aircraft's altitude during each of the first four aircraft encounters relative to the imagery-derived vertical extent (i.e., altitude of the top and bottom) of the ground cloud. It is apparent from this figure that the aircraft sampled at approximately the same altitude for the first two passes and climbed in altitude for next two passes. All of these aircraft encounters are within the lower portion of the imagery-defined vertical extent of the ground cloud. Upon review of Figures 7 and 8, one can conclude that the first four passes went through the lower portion of the southern lobe of the ground cloud.

This completes the 3D picture of the ground cloud for the first 10 min after launch. The 3-D picture includes not only the horizontal and vertical extent of the cloud but also the average concentration for each aircraft transit through the middle portion of the cloud. At times greater than 6 min, the aircraft is the only source of cloud data.

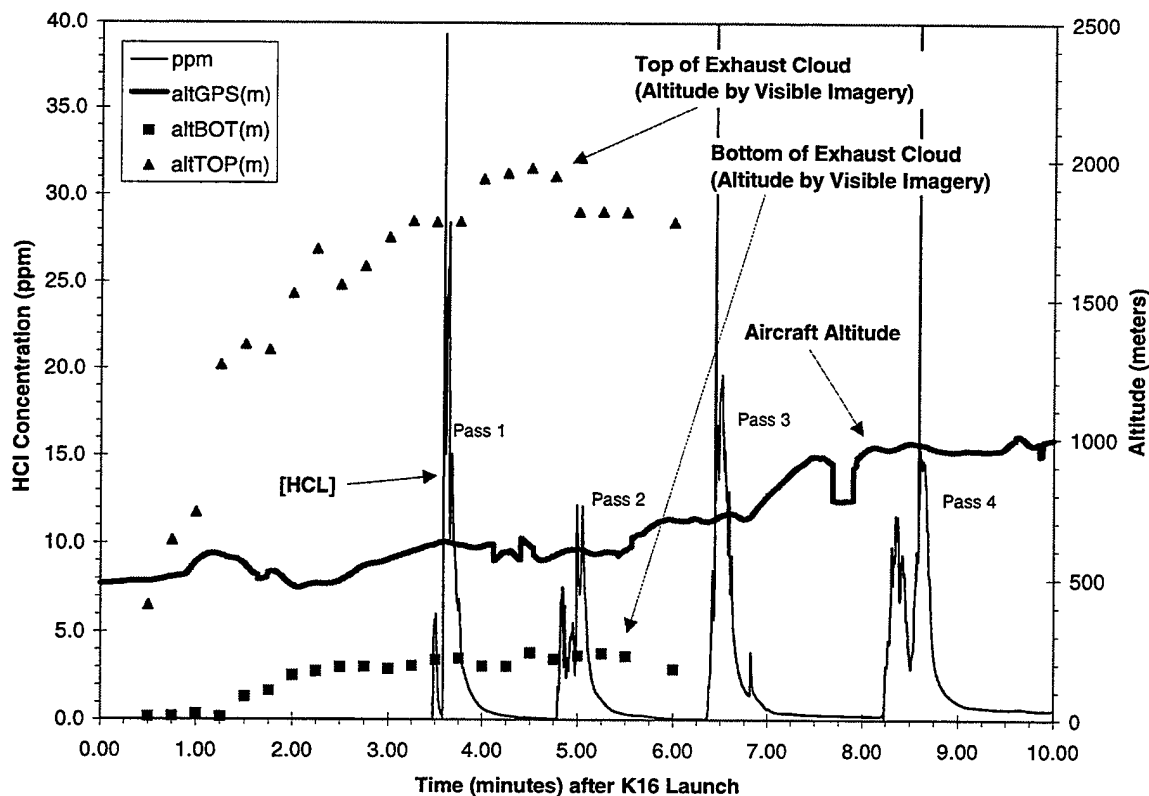


Figure 18. Altitude plot for aircraft and exhaust cloud (T = 0 to 10 min) with HCl Data.

3.2 Detailed Plots of Aircraft-Derived HCl Profiles (10-min Intervals)

The previous section of the results provided a 3-D picture of the ground cloud based upon the combination of quantitative imagery of the entire exhaust cloud and aircraft transits through portions of the exhaust cloud. The imagery-derived extent of the cloud provided an outline of the cloud and allowed the interpretation of the aircraft's Geomet-derived HCl concentrations as transits through the lower portion of the southern lobe of the ground cloud. There is no quantitative imagery for times longer than 6 min, but the aircraft sampled the ground cloud for 88 min. Therefore, one needs to analyze the aircraft data to determine its utility for mapping of the ground cloud trajectory and extent without complimentary imagery.

Appendix B contains two plots for each 10 min of aircraft data (i.e., 0–10, 10–20, through 80–90 min). The two plots provided for each 10 min of flight are:

- (1) A time plot documenting the aircraft altitude and the strength of the Geomet's HCl measurements (also, when available, the imagery-derived altitudes for the top and bottom of the ground cloud), and
- (2) A Cartesian plot documenting the location and the strength of the Geomet's HCl measurements.

Table 2 refers to the data plotted in Appendix B and provides data characteristic of each aircraft transit through the ground cloud (i.e., only the first 9 passes). The table lists the transit number (i.e., pass number) in the first column. Table 2 provides several characteristics for the maximum HCl hit for each pass, including: elapsed time after launch (column 2), the peak HCl concentration (column 3), the sampling altitude (column 4), and the aircraft's polar location (i.e., distance in column 6 and angle in column 7). Table 2 also lists the plume-to-pad distance (column 8) calculated using the time (column 2) and the imagery-derived average ground cloud speed (i.e., 3.6 m/s). Comparison of the column 8 distance to the column 6 distance reveals that the aircraft flew through the far end of the cloud for most of these encounters (i.e., column 6 > column 8). For passes 1–4, this was shown to be true in the previous section of the results where the imagery-derived extent was compared to the aircraft's flight data. Table 2 provides a qualitative description of the type of pass in column 5 and a rough estimate of the polar extent of the cloud (i.e., the difference in distance in column 9 and the difference in angle in column 10 between the first and last hit for each transit).

The aircraft's polar angular location (i.e., column 7) is reported in rawinsonde convention for comparison to wind angles. An angle of 360° indicates an aircraft location to the South (i.e., with a wind from the North). An angle of 90° indicates an aircraft location to the West (i.e., with a wind from the East and perpendicular to a wind from the North).

The maximum hits for Passes 1–3 and 9 are in the southwest quadrant (i.e., 1° to 38° in column 7) while the other hits are in the southeast quadrant (i.e., 357° to 297° in column 7). The imagery documented that the lower end of the ground cloud went to the southwest and therefore only passes 1–3 and 9 are consistent with sampling the distant end of the ground cloud. The other hits follow the higher altitude portions of the ground cloud and possibly the launch column that moved out to sea. The aircraft continued to move up in altitude and out to sea and, therefore, concentrated on the higher altitude portion of the ground cloud or possibly the launch column. Table 2 includes only the lower altitude ground cloud data collected at early times. The imagery documented that the lower portion of the ground cloud continued to the southwest throughout the 55 min of imaging. The figures in Appendix B and the figures in the next section characterize all of the aircraft data.

Table 2. Summary of Aircraft-Derived Ground Cloud Information

No.	Time of Pass	Peak HCl	Sampling Altitude	Type of Pass ¹	Aircraft Location w.r.t. SLC-41		Plume to Pad ²	Plume Parameters	
	at max.	at max.	at max.		at max.			ΔD	$\Delta \theta$
	(min)	(ppm)	(meters)		$\Delta(m)$	$\theta(^{\circ})$	(m)	(m)	($^{\circ}$)
1	3.50	6.0	623	Downwind	1405	38	756	837	52
2	4.99	12.1	606	Upwind	2041	15	1078	745	55
3	6.51	19.6	726	Crosswind	2344	17	1406	786	52
4	8.61	15.4	979	Crosswind	2278	357	1860	108	65
5	10.96	23.7	981	Crosswind	3265	342	2367	1713	32
6	12.35	8.2	1031	Downwind	3921	328	2668	917	26
7	14.55	11.7	1089	Upwind	3428	350	3143	2119	16
8	16.67	6.6	1284	Downwind	3629	297	3601	584	56
9	20.03	2.7	848	Crosswind	5339	1	4326	3111	25

¹The terms "crosswind" and "downwind" are used as relative labels and are not exact.

²The plume to pad distance was calculated using the imagery derived average wind speed (3.6 m/s).

The analyst did not correct for any lag time for the start of response or the start of fall. It is reasonable to assume that the lag time is symmetrical (i.e., the same for the start and fall). Therefore, the length of the pass (i.e., the extent of the cloud) should be reasonably accurate. The lag time is probably 1 or 2 s and was not measured by INET.

The data presented earlier in Figures 9–17 documented the extent of the cloud (i.e., horizontal line) used to calculate the average concentration as well as the extent of the data (i.e., full duration of plot) used to integrate the total dosage. It is important to understand that the start and end of the pass are intended to map the main portion of the cloud and not the slow recovery of the Geomet after leaving the cloud. For the plots in Figures 9–17, the start and end of the cloud was determined solely by the initial response and by the end of rapid fall, respectively. No geometrical restrictions applied.

The analyst used some geometrical bias to determine the plume parameters reported in Table 2. If the bulk of the hits were along a straight course, but the aircraft started its turn before the exiting the cloud, the analyst picked the last hit along the straight course so the start and end mapped the direction of travel and the extent of the cloud.

3.3 Summary Plots of Aircraft Geomet HCl Data (88-min Interval)

The previous sections and Appendix B graphically documented and parameterized the available data in great detail for limited periods of the flight. This portion of the results uses graphical methods to summarize the aircraft data for the entire mission. Several of these plots were included in the previous report⁵ and are included here as a convenience to the reader.

This series of plots graphically document the entire HCl dataset (i.e., Figures 19 through 23). Figure 19 is a Cartesian plot of the flight trajectory labeled to reveal the distribution of HCl sampling data. The remaining figures (i.e., 20 through 23) are time plots that document the aircraft-derived HCl concentrations. In addition to the HCl concentration, Figure 20 includes the polar angle to each sampling, Figure 21 includes the polar ground distance to each sampling, Figure 22 includes the altitude (m MSL) for each sampling; and Figure 23 includes the effective cloud speed needed to reach the position of the sampling. These various parameters were included to illustrate the complexity of the dataset and to provide all of the data needed for comparison with models.

Review of these figures reveals that the aircraft only sampled the lower-altitude southwestern regions of the ground cloud at early (i.e., <20 min) and late (i.e., >74 min) times. Likewise, the data indicate that higher effective cloud speeds were only probed at early and late times. These results are consistent with limited sampling of the portion of the ground cloud that moved inland. Therefore, most of the aircraft's data concentrate on the higher altitude portion of the ground cloud or possibly the launch column that moved to the east-southeast of the launch pad.

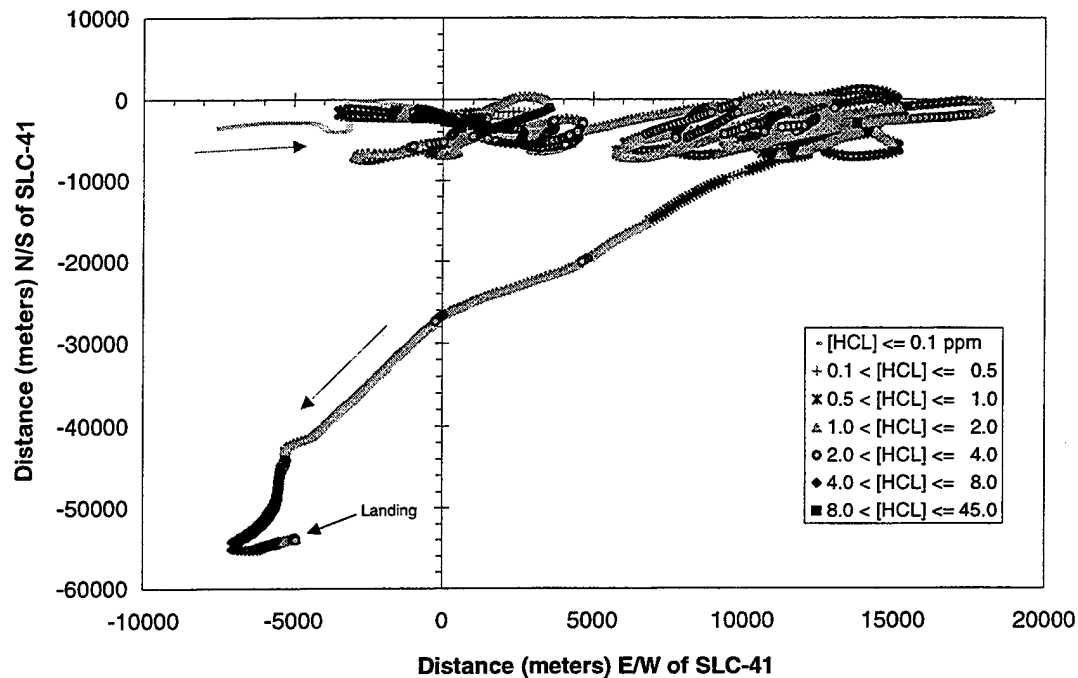


Figure 19. Cartesian position labeled with HCl concentration (0 to 90 min).

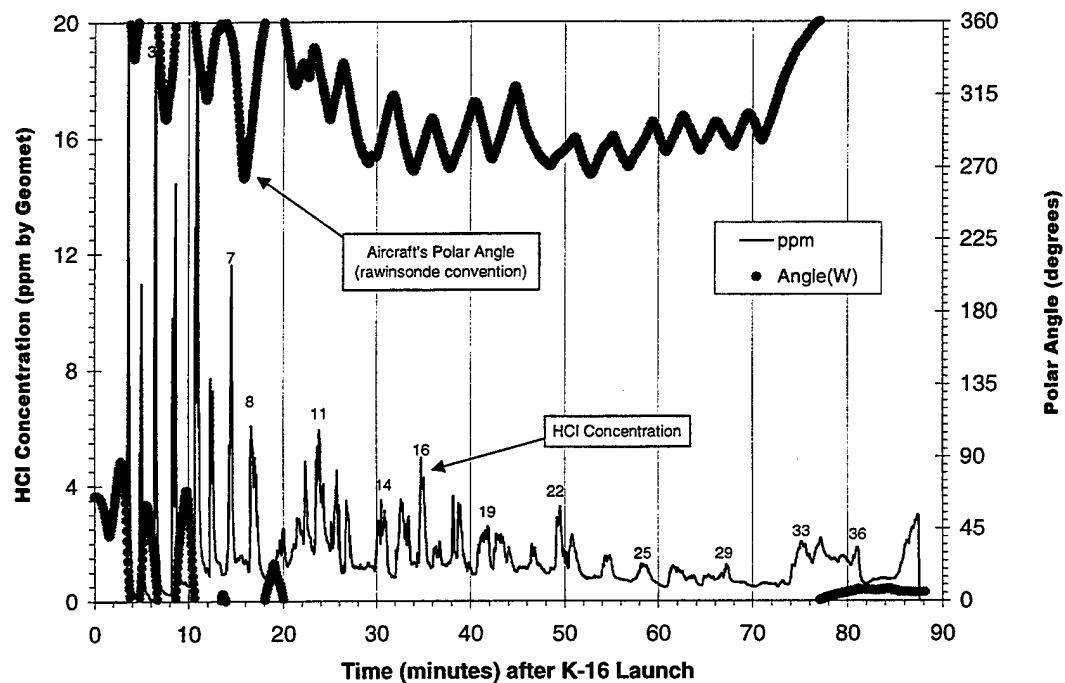


Figure 20. Polar angle and HCl concentration plotted against time (0 to 90 min).

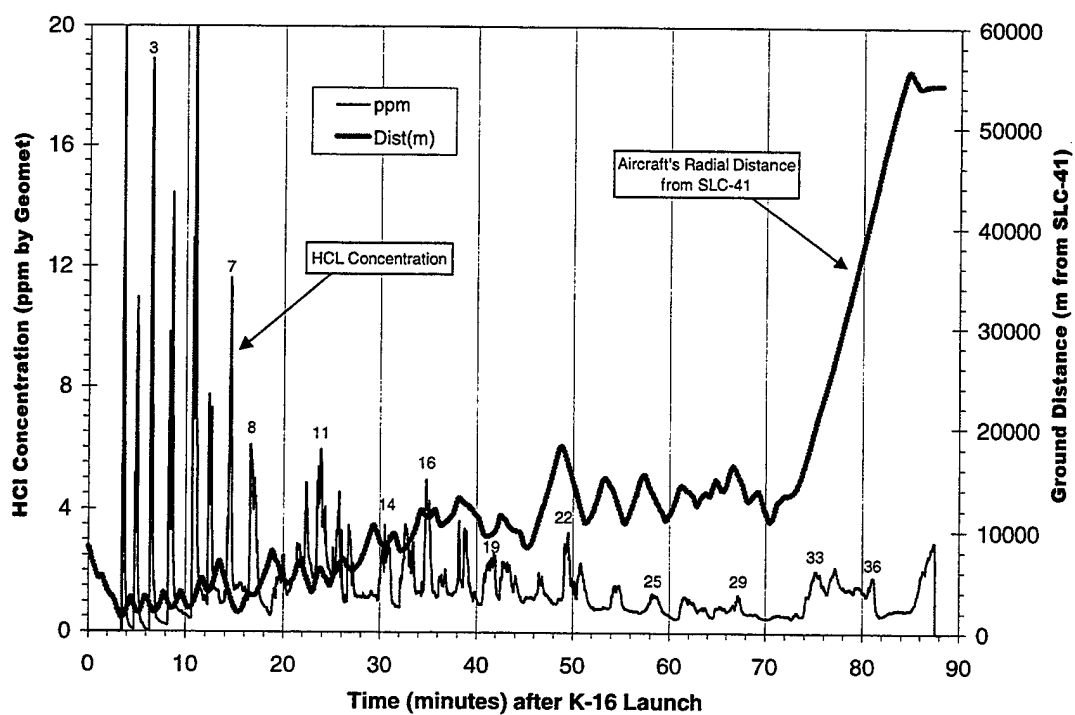


Figure 21. Ground Distance and HCl concentration plotted against time (0 to 90 min).

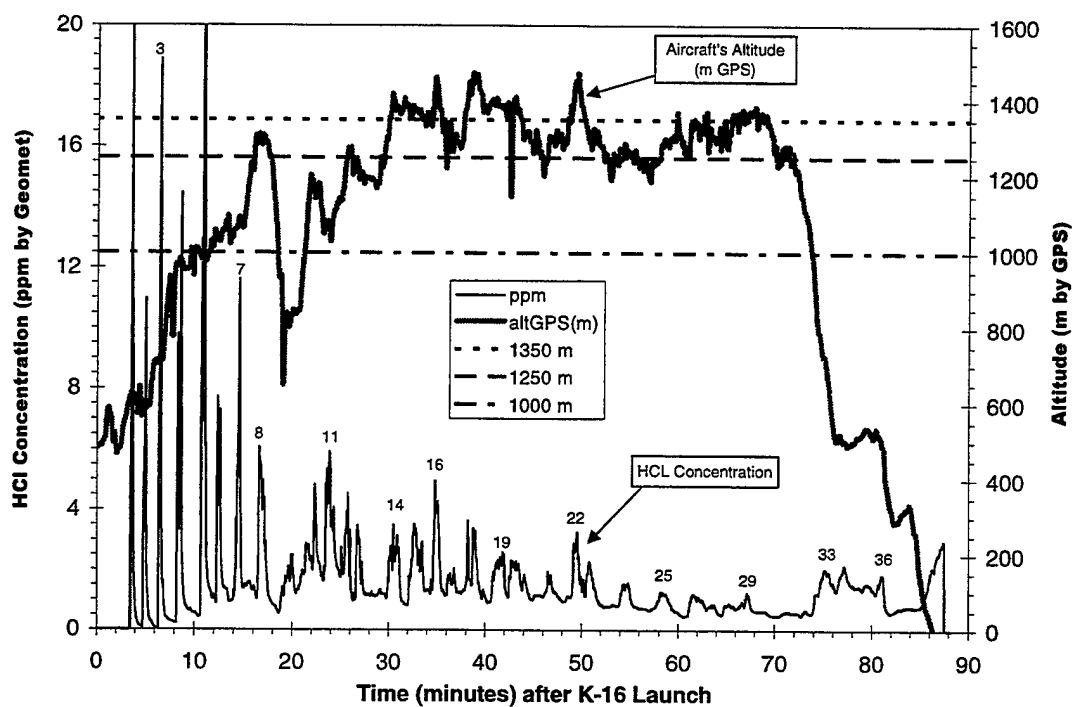


Figure 22. Altitude and HCl concentration plotted against time (0 to 90 min).

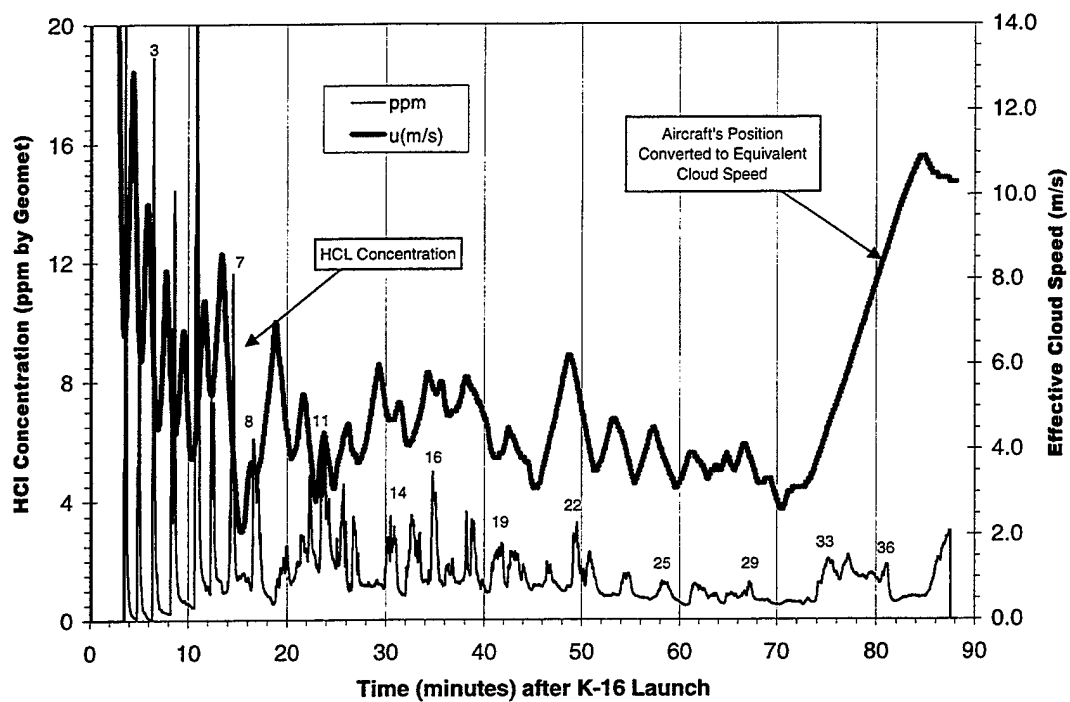


Figure 23. Effective speed and HCl concentration plotted against time (0 to 90 min).

4. Conclusions

The combination of the visible imagery with aircraft sampling provided a three-dimensional picture of the Titan IV #K16 exhaust cloud for the first 6 min after launch. Since the ground cloud over-filled the FOV within the first 6 min, we did not process the later imagery quantitatively. However, qualitatively, the entire 55 min of imagery documented the movement of the lower portion of the cloud to the south-southwest and the shearing of the launch column to the east. The aircraft sampled various portions of the ground cloud and launch column during the 88 min immediately following launch.

Review of the aircraft and imagery data revealed consistent edge detection by the quantitative imagery and by the aircraft's HCl monitor. The imagery documented that the aircraft sampled the distant portion of the ground cloud during its first three encounters. The aircraft only sampled the southern low-altitude lobe of the ground cloud a couple of more times (i.e., passes 4 and 9) before climbing into the higher altitude launch column, which moved out to sea. Finally the aircraft detected low-altitude HCl hits once again as it passed through the southwestern quadrant on its return to the airport. These later data are consistent not only with the imagery-derived initial bearing of the lower altitude portion of the ground cloud but also with the entire 55 min of imagery. In summary, the aircraft collected some data in the lower portion of the ground cloud but concentrated mainly upon the higher altitude portions that moved out to sea.

It is important to remember that the aircraft's Geomet detector mapped regions of HCl concentration as well as regions not occupied by the exhaust cloud. It is important to compare model predictions not only to the measured HCl concentrations within the cloud but also to the zero concentrations outside of the cloud. To this end, the aircraft's data is available in electronic form. This will allow rigorous comparison to model predictions using the aircraft's sampling positions as point receptors (i.e., latitude, longitude, altitude, and time). Three-dimensional plotting can also be used to compare model predictions to aircraft measurements.

References

1. Environmental Systems Directorate, "Ground Cloud Dispersion Measurements During the Titan IV #K23 (14 May 1995) at Cape Canaveral Air Force Station: Volume 1—Test Overview and Data Summary," Aerospace Report No. TR-96(1410)-1, SMC-TR-96-01, The Aerospace Corporation, El Segundo, CA (27 February 1996).
2. Environmental Systems Directorate, "Ground Cloud Dispersion Measurements During the Titan IV #K19 (10 July 1995) at Cape Canaveral Air Force Station," Aerospace Report No. TR-96(1410)-3, SMC-TR-96-18, The Aerospace Corporation, El Segundo, CA (22 March 1996).
3. Environmental Systems Directorate, "Ground Cloud Dispersion Measurements During the Titan IV #K21 (6 November 1995) at Cape Canaveral Air Force Station," Aerospace Report No. TR-96(1410)-4, SMC-TR-96-21, The Aerospace Corporation, El Segundo, CA (21 June 1996).
4. Environmental Systems Directorate, "Ground Cloud Dispersion Measurements During The Titan IV Mission #K15 (24 April 1996) at Vandenberg Air Force Base, Volume 1—Test Overview and Data Summary," Aerospace Report No. TR-97(1410)-3, SMC-TR-97-05, The Aerospace Corporation, El Segundo, CA (10 February 1997).
5. Environmental Systems Directorate, "Ground Cloud Dispersion Measurements During the Titan IV #K16 (24 April 1996) at Cape Canaveral Air Force Station, Volume 1—Test Overview and Data Summary," Aerospace Report No. TR-97(1410)-4, SMC-TR-97-10, The Aerospace Corporation, El Segundo, CA (31 March 1997).
6. Environmental Systems Directorate, "Ground Cloud Dispersion Measurements During the Titan IV #K22 (12 May 1996) at Vandenberg Air Force Base, Volume 1—Test Overview and Data Summary," Aerospace Report No. TR-97(1410)-5, SMC-TR-97-18, The Aerospace Corporation, El Segundo, CA (30 June 1997).
7. Environmental Systems Directorate, "Ground Cloud Dispersion Measurements During the Titan IV Mission #K2 (3 July 1996) at Cape Canaveral Air Force Station, Volume 1—Test Overview and Data Summary," Aerospace Report No. TR-97(1410)-6, SMC-TR-97-19, The Aerospace Corporation, El Segundo, CA (15 July 1997).
8. Environmental Systems Directorate, "Ground Cloud Dispersion Measurements During the Titan IV Mission #K24 (23 February 1997) at Cape Canaveral Air Force Station, Volume 1—Test Overview and Data Summary," The Aerospace Corporation Report No. TR-97(1410)-7, SMC-TR-98-01, The Aerospace Corporation, El Segundo, CA (10 October 1997).
9. Environmental Systems Directorate, "Ground Cloud Dispersion Measurements During the Titan IV Mission #K13 (20 December 1996) at Vandenberg Air Force Base, Volume 1—Test

- Overview and Data Summary," The Aerospace Corporation Report No. TR-97(1410)-8, SMC-TR-98-02, The Aerospace Corporation, El Segundo, CA (10 October 1997).
10. Environmental Systems Directorate, "Ground Cloud Dispersion Measurements During the Titan IV Mission #B33 (15 October 1997) at Cape Canaveral Air Force Station," The Aerospace Corporation Report No. TR-98(1410)-3, SMC-TR-98-31, The Aerospace Corporation, El Segundo, CA (30 June 1998).
 11. Environmental Systems Directorate, "Ground Cloud Dispersion Measurements During the Titan IV Mission A-18 (23 October 1997) at Vandenberg Air Force Base," The Aerospace Corporation Report No. TR-99(1413)-3, SMC-TR-99-14, The Aerospace Corporation, El Segundo, CA (20 February 1999).
 12. Environmental Systems Directorate, "Ground Cloud Dispersion Measurements During the Titan IV Mission A-17 (7 November 1997) at Cape Canaveral Air Force Station," The Aerospace Corporation Report No. TR-99(1413)-2, SMC-TR-99-15, The Aerospace Corporation, El Segundo, CA (20 February 1999).
 13. R. N. Abernathy, R. F. Heidner III, B. P. Kasper, and J. T. Knudtson, "Visible and Infrared Imagery of the Launch of Titan IV K-23 from Cape Canaveral Air Force Station on 14 May 1995," Aerospace Report No. TOR-96(1410)-1, The Aerospace Corporation, El Segundo, CA (15 September 1996).
 14. R. N. Abernathy and K. L. Foster, "Ground Cloud Dispersion Measurements During The Titan IV Mission #K15 (5 December 1995) at Vandenberg Air Force Base; Volume 2—Further Analysis of Quantitative Imagery and of Aircraft HCl Data," The Aerospace Corporation Technical Report TR-98(1410)-2, The Aerospace Corporation, El Segundo, CA (12 May 1998).
 15. R. N. Abernathy, R. F. Heidner III, and K. L. Foster, "Aircraft HCl Sampling of the Titan IV K-23 Launch Effluent Cloud," Aerospace Report No. TR-96(1410)-2, SMC-TR-96-22, The Aerospace Corporation, El Segundo, CA (15 September 1996).
 16. R. N. Abernathy, "Titan 34D-9 Abort Cloud Measurements—Quantitative Imagery from Two Camera Sites," Aerospace Report No. TR-98(1410)-1, The Aerospace Corporation, El Segundo, CA (20 February 1998).
 17. R. N. Abernathy, I. A. Min, B. L. Lundblad, and W. S. Kempf, "Tracer Puff Dispersion at Launch Sites" The Aerospace Corporation Report No. TR-99(1413)-4, SMC-TR-99-25, The Aerospace Corporation, El Segundo, CA (15 July 1999).

Appendix A—Acronyms and Abbreviations

AGL	Above Ground Level (SLC-41 is ground level for #K16)
Alt	Altitude in meters above mean sea level (MSL)
AZ	Azimuth clockwise from north
CCAFS	Cape Canaveral Air Force Station
dAZ	Difference in AZ between two objects in an image
dEL	Difference in EL between two objects in an image
dW	Difference in absolute Width (i.e., corrected for FOV) for an object observed in different images
dX	Difference in X pixel values between two pixels (i.e., objects in an image)
dY	Difference in Y pixel values between two pixels (i.e., objects in an image)
D	ground Distance between two objects
EDT	Eastern Daylight Time
EL	Elevation of object relative to level
FOV	Field Of View of image in degrees horizontal or degrees vertical
GMT	Greenwich Mean Time
Ground Cloud	normal launch cloud that includes exhaust reflected from pad and launch column consumed by rising exhaust duct cloud
LBS	pounds
mean	weighted average of all values
middle	half way between the top and the bottom and half way between the left and the right
MSL	Mean Sea Level is the reference used for all altitudes in this report
MST	Mobile Service Tower at launch pad
MVP	Model Validation Program
N ₂ O ₄	dinitrogen tetroxide (i.e., hypergolic oxidizer)
PSIA	Pounds per Square Inch Absolute
REEDM	Rocket Exhaust Effluent Dispersion Model used at VAFB and CCAFS
SLC	Space Launch Complex
SR	Slant Range between imagery site and observed feature
SRM	Solid Rocket Motor
TVC	Thrust Vector Control
UT	Umbilical Tower at launch pad

VAFB	Vandenberg Air Force Base
x	Cartesian coordinate in east/west direction relative to SLC-41 at x,y = 0,0
X	"horizontal" pixel value (i.e., 0 at left of image and 640 at right of image)
y	Cartesian coordinate in north/south direction relative to SLC-41 at x,y = 0,0
Y	"vertical" pixel value (i.e., 0 at bottom of image and 480 at top of image)
z	altitude relative to MSL (opposed to "Alt" which is relative to SLC-41)

Appendix B—10-Min Plots for Aircraft Data

The following figures document the aircraft's position and the Geomet's HCl measurements using two plots for each 10-min period. During the first 6 min after launch, the quantitative imagery of the entire exhaust cloud was combined with the aircraft transits through portions of the exhaust cloud to generate a 3-D picture of the ground cloud. As discussed in the results section of this report, the imagery-derived extent of the cloud provided an outline of the cloud and allowed the interpretation of the aircraft's early Geomet-derived HCl concentrations as transits through the middle portion of the ground cloud. There is no quantitative imagery for times longer than 6 min, but the aircraft sampled the ground cloud for 88 min. The discussion in the body of the report established that the aircraft sampled the lower portion of the ground cloud only at very early (<20 min) and, possibly, at late times (>74 min). The bulk of the aircraft data applies to the high-altitude portion of the launch cloud (possibly the launch column) that sheared to the east after launch.

As discussed in the results section of this report, Appendix B contains two plots for each 10 min of aircraft data (i.e., 0–10, 10–20, through 80–90 min). The two plots provided for each 10 min of flight are:

- A time plot documenting the aircraft altitude and the strength of the Geomet's HCl measurements (also, when available, the imagery-derived altitudes for the top and bottom of the ground cloud)
- A Cartesian plot documenting the location and the strength of the Geomet's HCl measurements.

The results' section discusses not only these plots but also provides additional tabular and graphical analysis of the aircraft data. As discussed in the results section of this report, there are electronic spikes that were recorded by the aircraft's data system. The rapid rise and fall (i.e., essentially vertical) associated with these electronic artifacts (i.e., possibly radio transmissions) allow one to differentiate them from the smoother Geomet response, which has a characteristic tail. Figure B-6 includes two small negative spikes (i.e., after pass 23 and on the tail of pass 25), one small positive spike (i.e., lead of pass 24), and one large positive spike (i.e., during pass 25). Most plots within this appendix contain at least one of these artifacts.

Since the Geomet can respond to oxidizing compounds and to other strong acids, landing at the airport may introduce another possible "artifact," that is, response to interfering compounds. Therefore, one cannot assert that the Geomet response after landing is due solely to the launch cloud. Unfortunately, we were not provided with detector response prior to take-off, during taxiing, and during ascent. Such data would have provided a useful baseline for interpreting the data collected during landing.

We provide these detailed plots to allow direct comparison with REEDM output. These data are available as ASCII comma-separated-variable files to facilitate more rigorous comparisons. This report is available electronically as a PDF file that can be viewed in color using ACROBAT[®] viewer (free over the Internet).

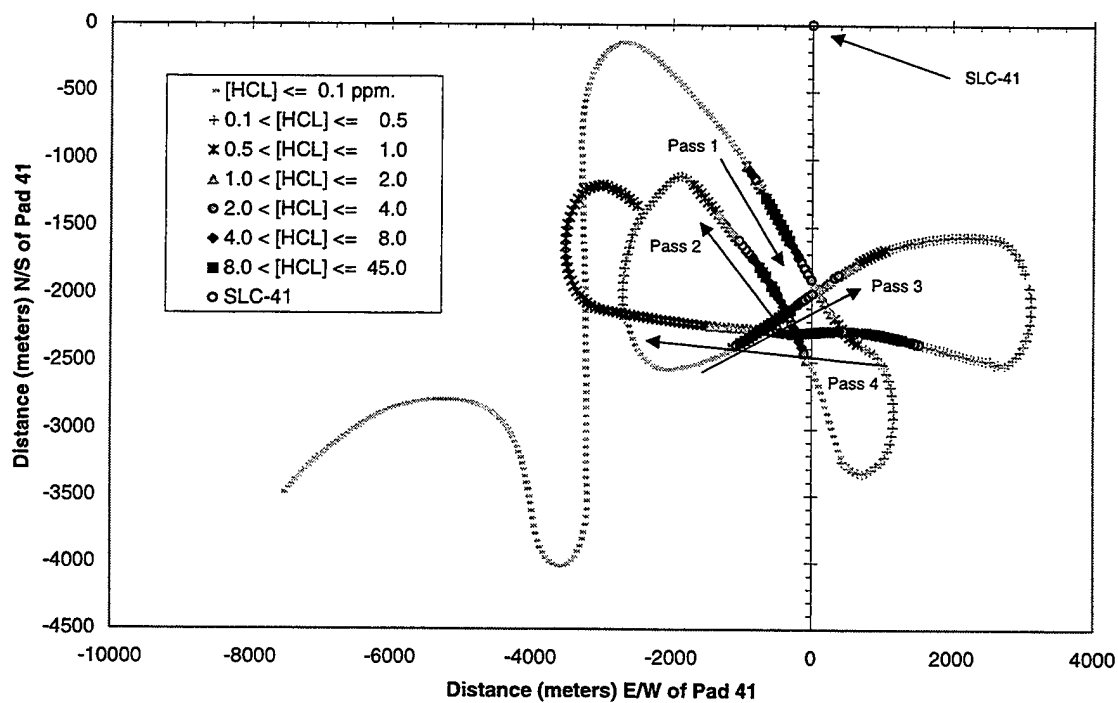
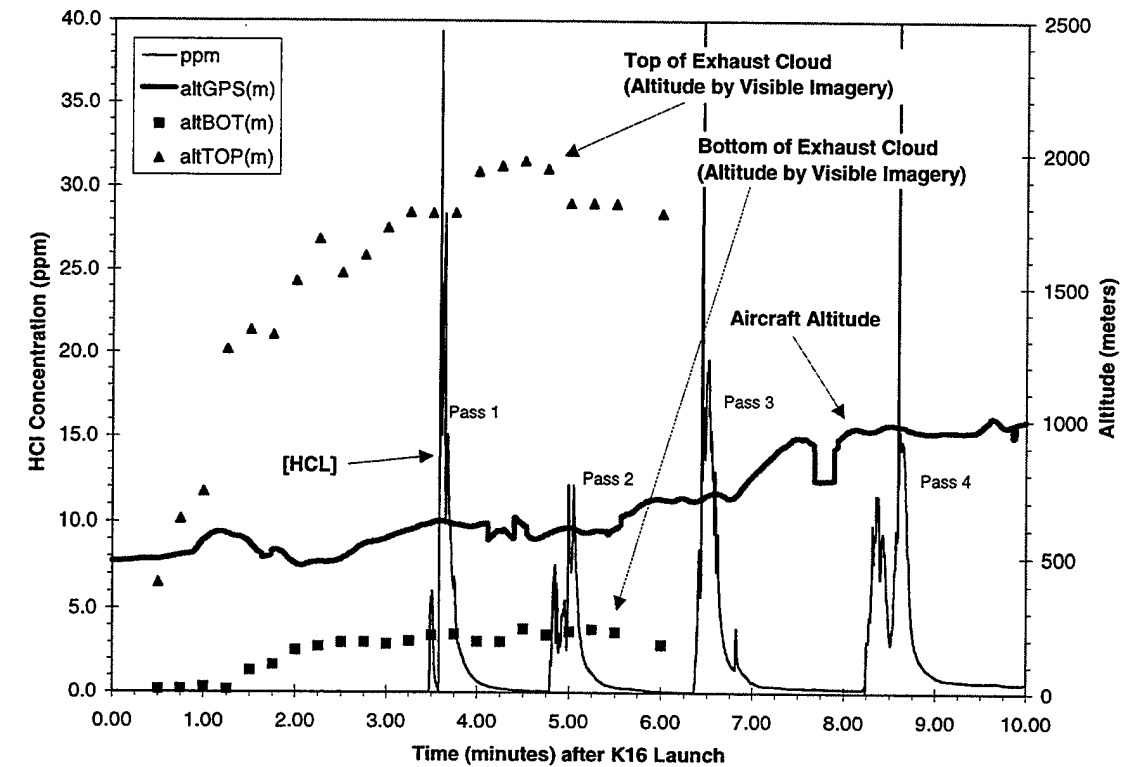


Figure B-1. Time and Cartesian plots for aircraft passes 1–4 (T = 0 to 10 minutes).

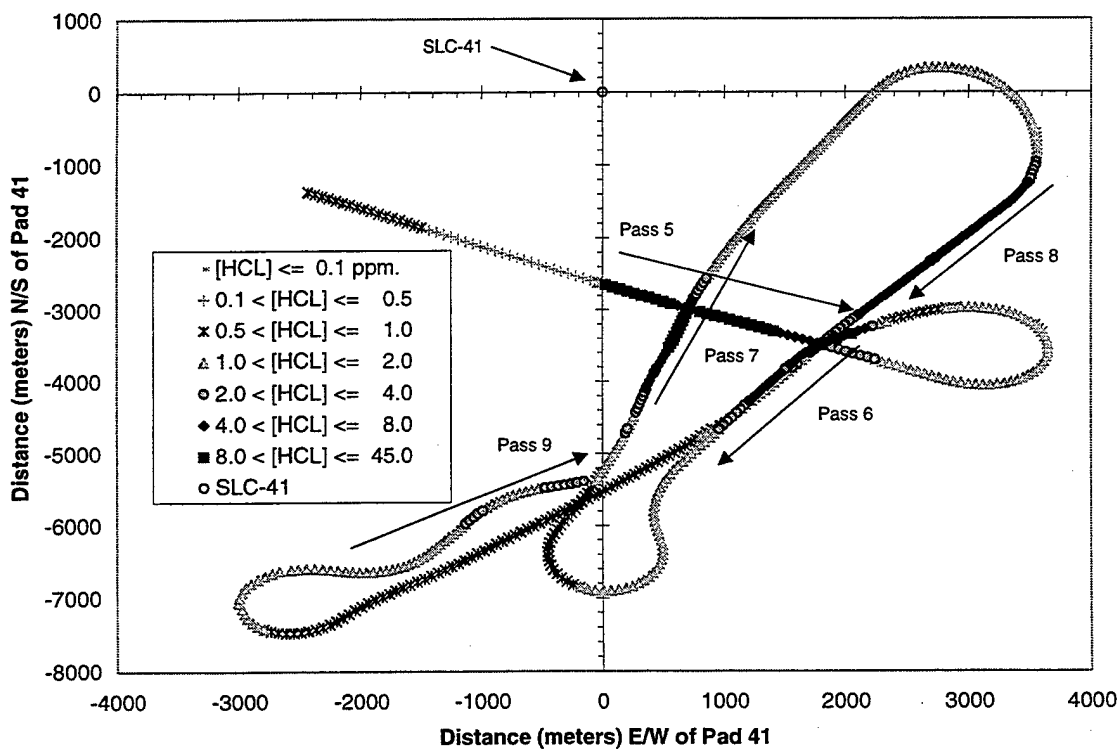
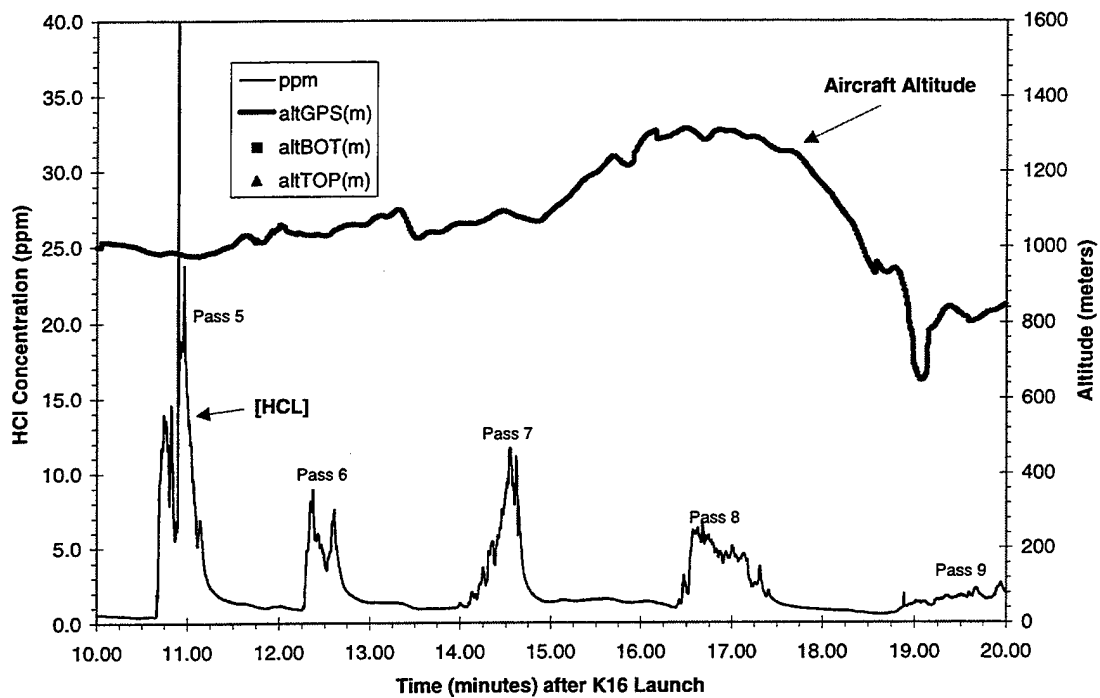


Figure B-2. Time and Cartesian plots for aircraft passes 5-9 (T = 10 to 20 minutes).

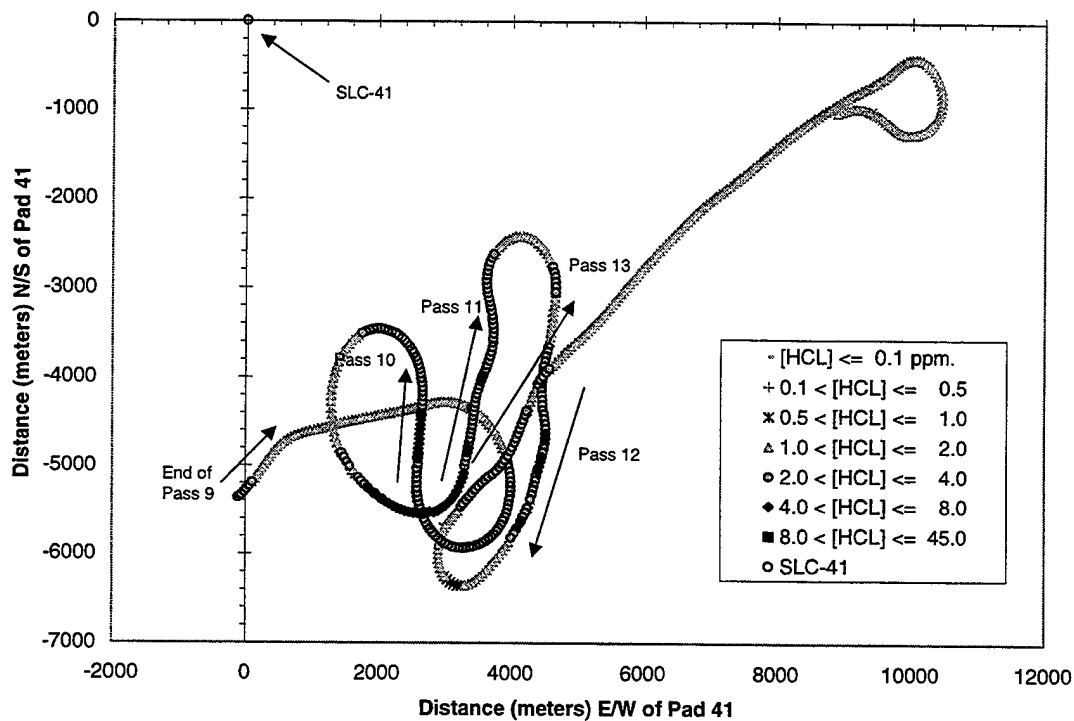
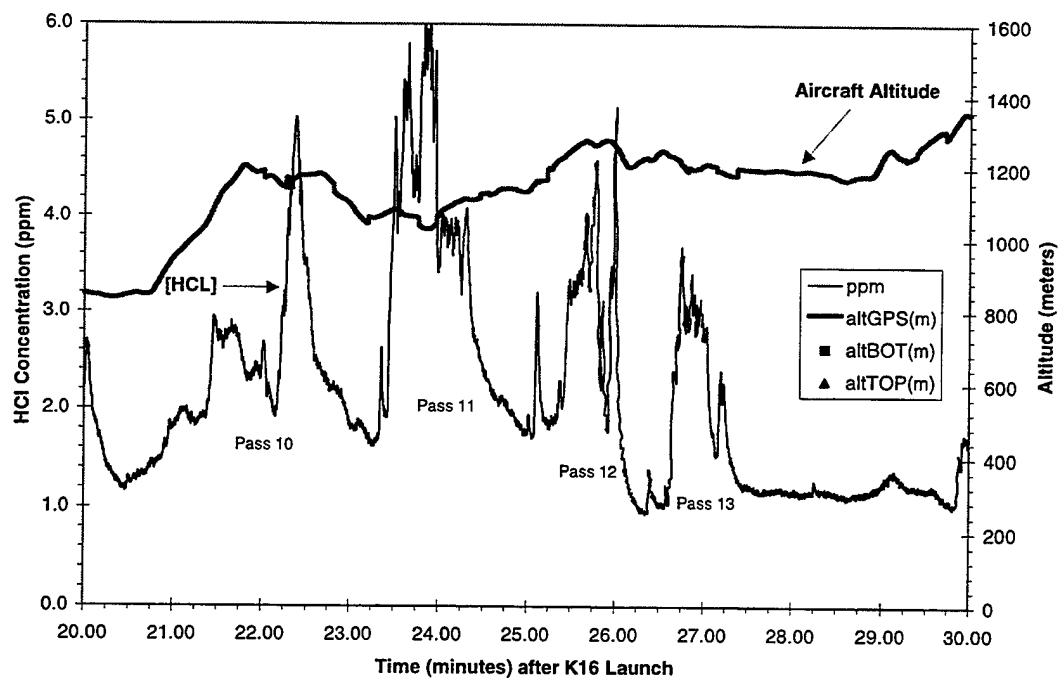


Figure B-3. Time and Cartesian plots for aircraft passes 10–13 (T = 20 to 30 minutes).

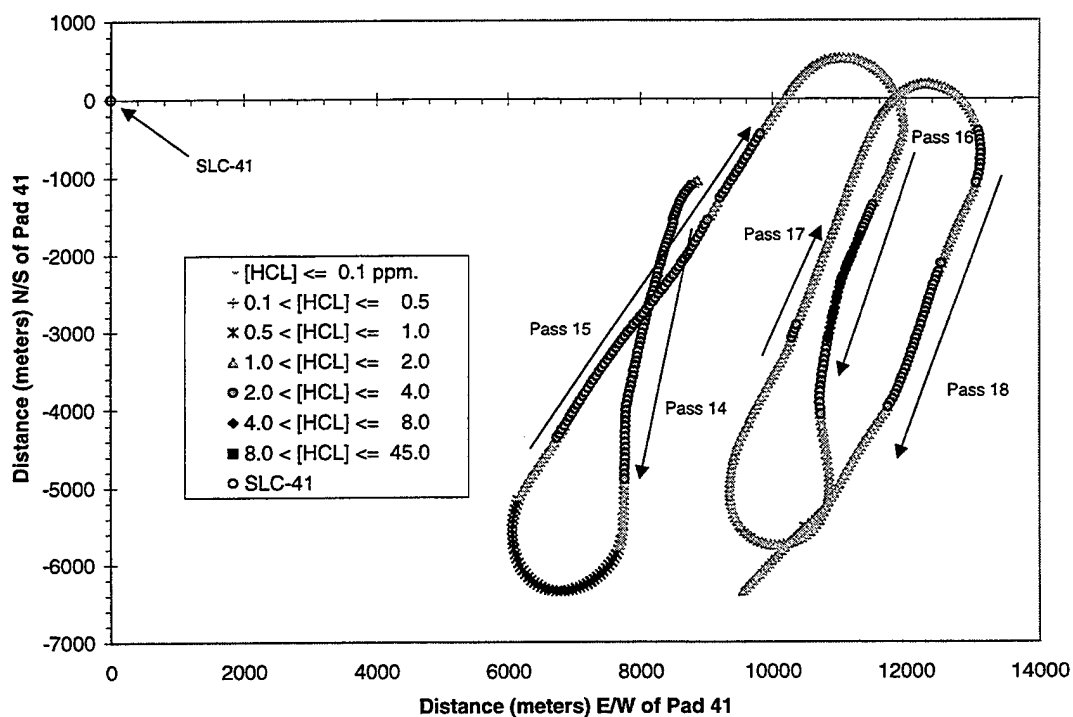
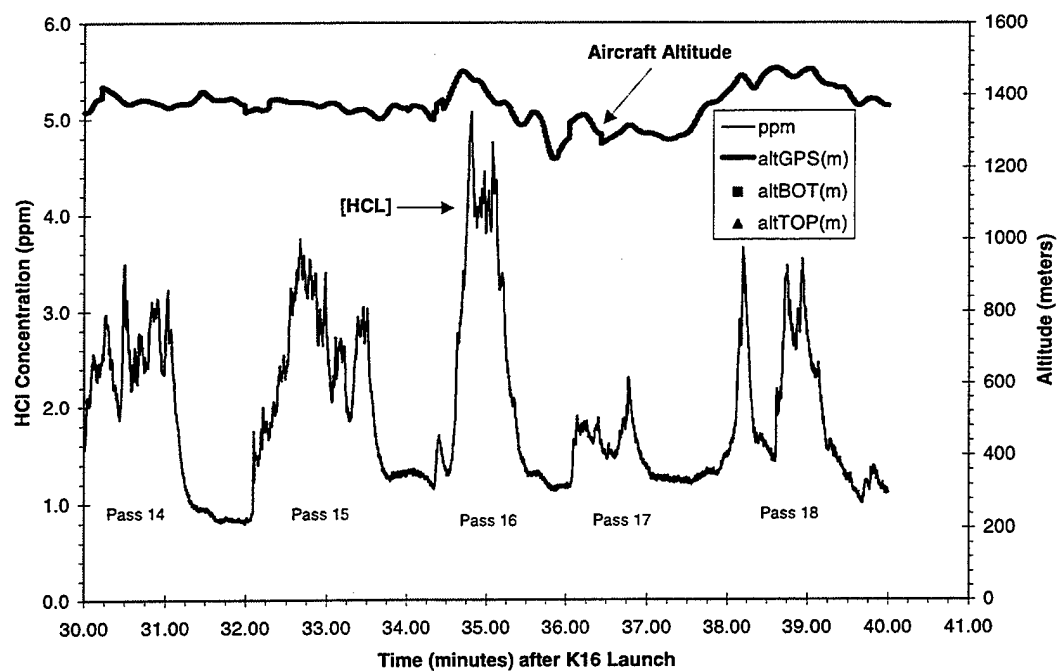


Figure B-4. Time and Cartesian plots for aircraft passes 14-18 (T = 30 to 40 minutes).

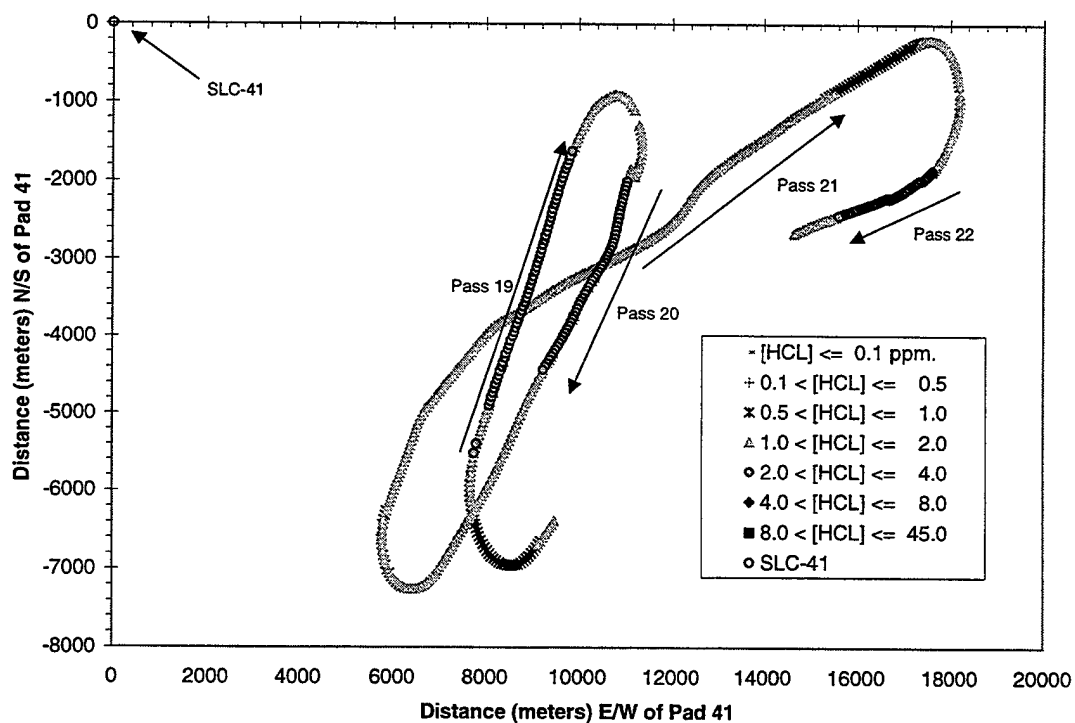
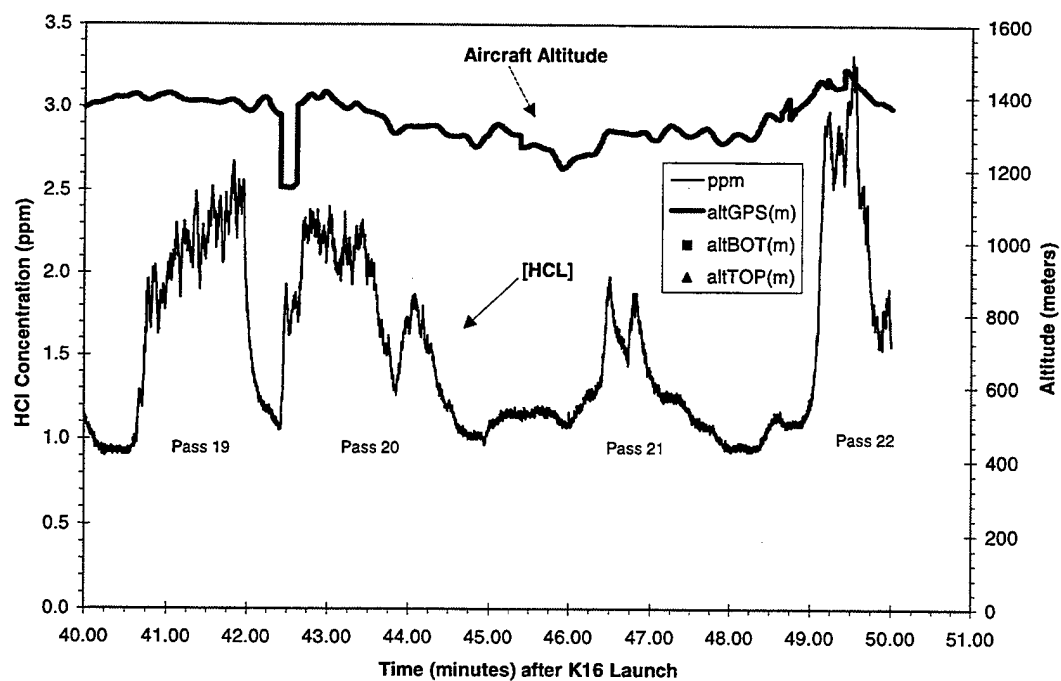


Figure B-5. Time and Cartesian plots for aircraft passes 19-22 (T = 40 to 50 minutes).

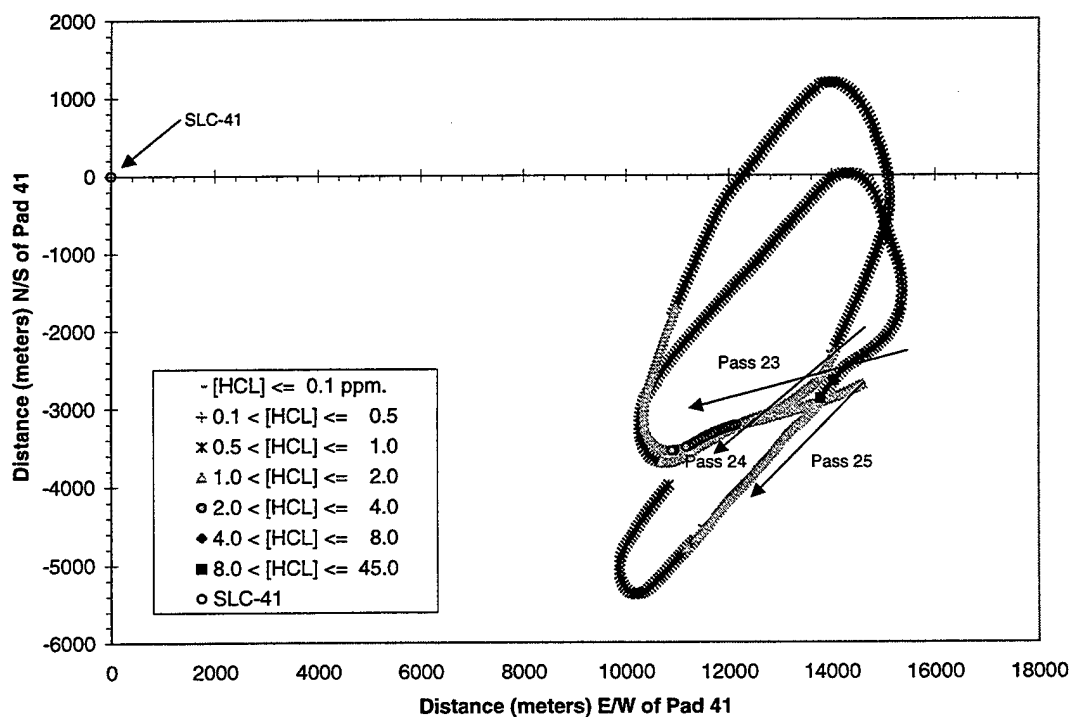
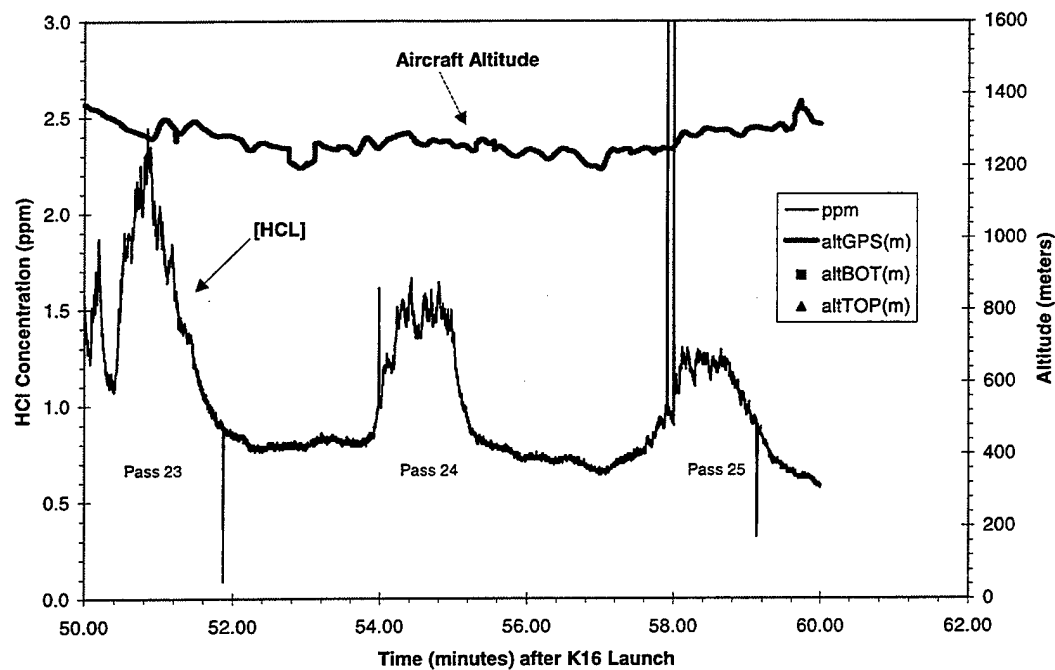


Figure B-6. Time and Cartesian plots for aircraft passes 23–25 (T = 50 to 60 minutes).

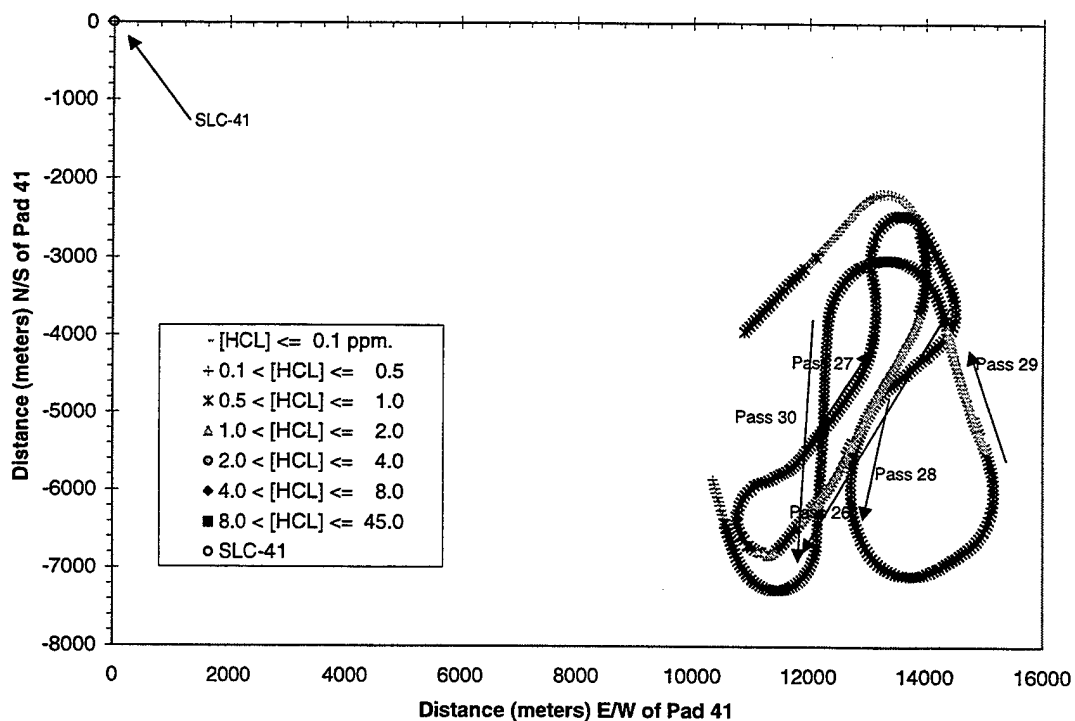
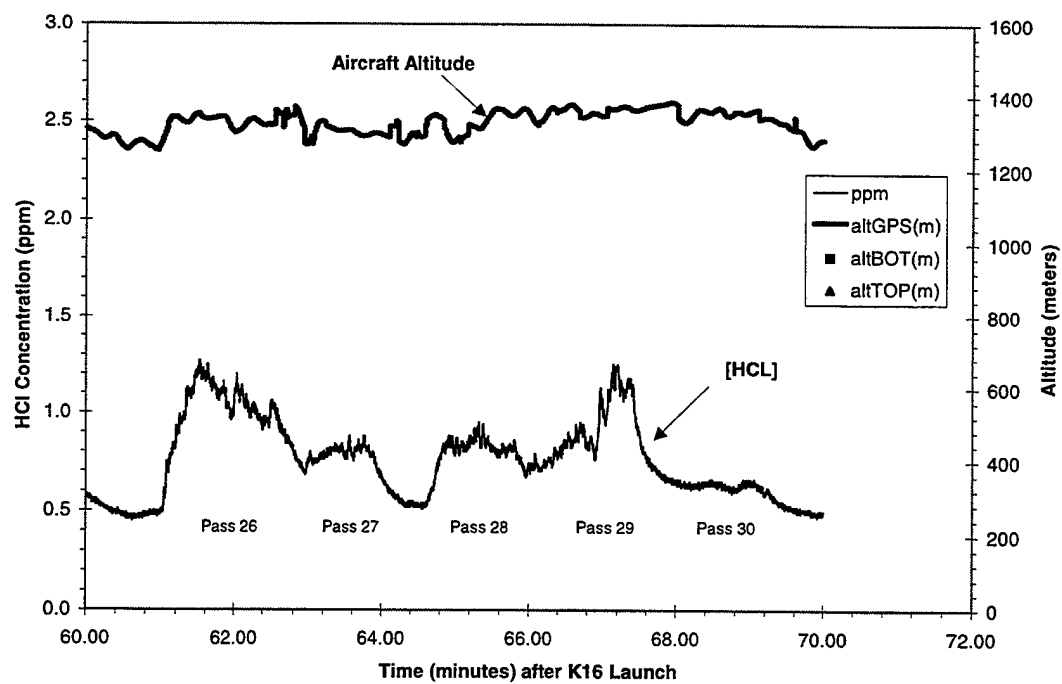


Figure B-7. Time and Cartesian plots for aircraft passes 26–30 (T = 60 to 70 minutes).

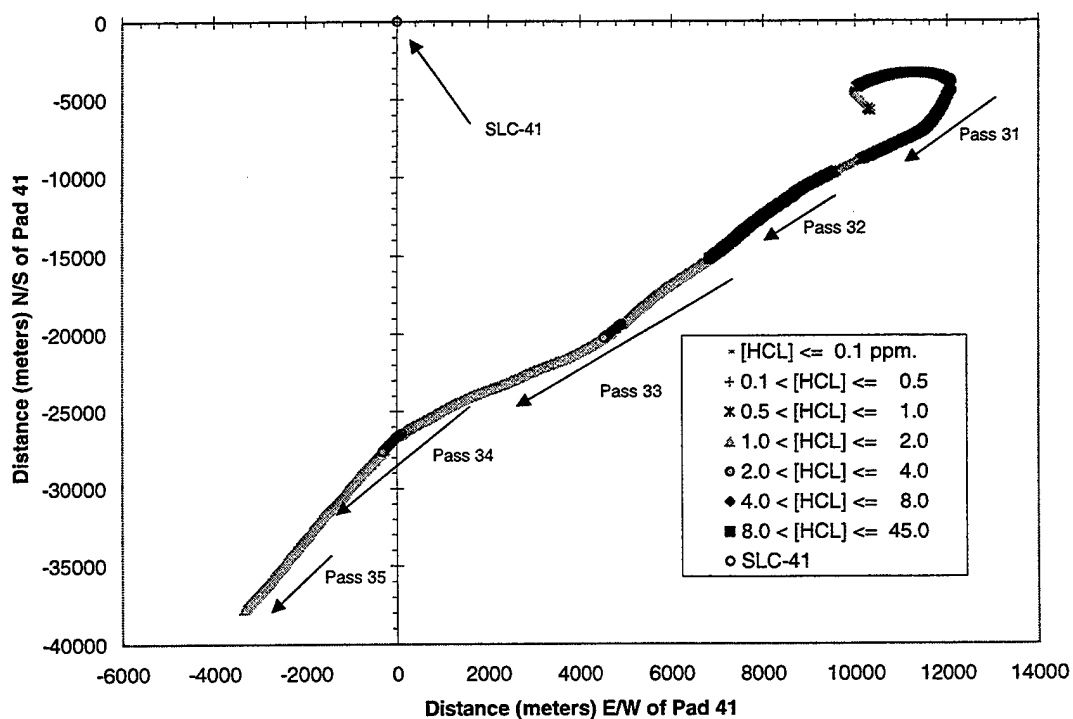
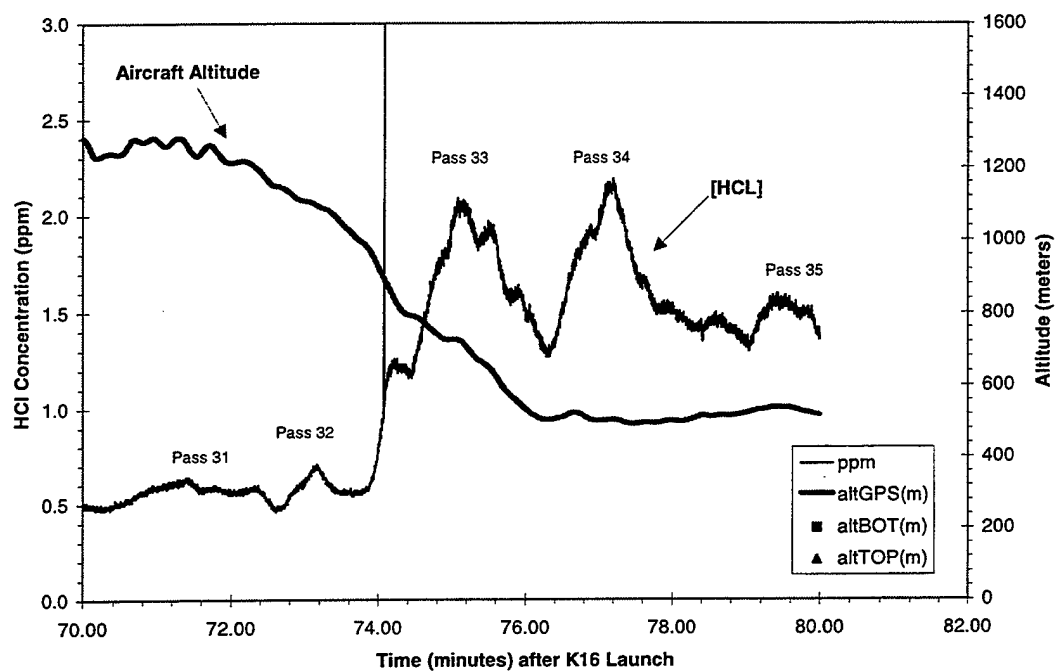


Figure B-8. Time and Cartesian plots for aircraft passes 31-35 (T = 70 to 80 minutes).

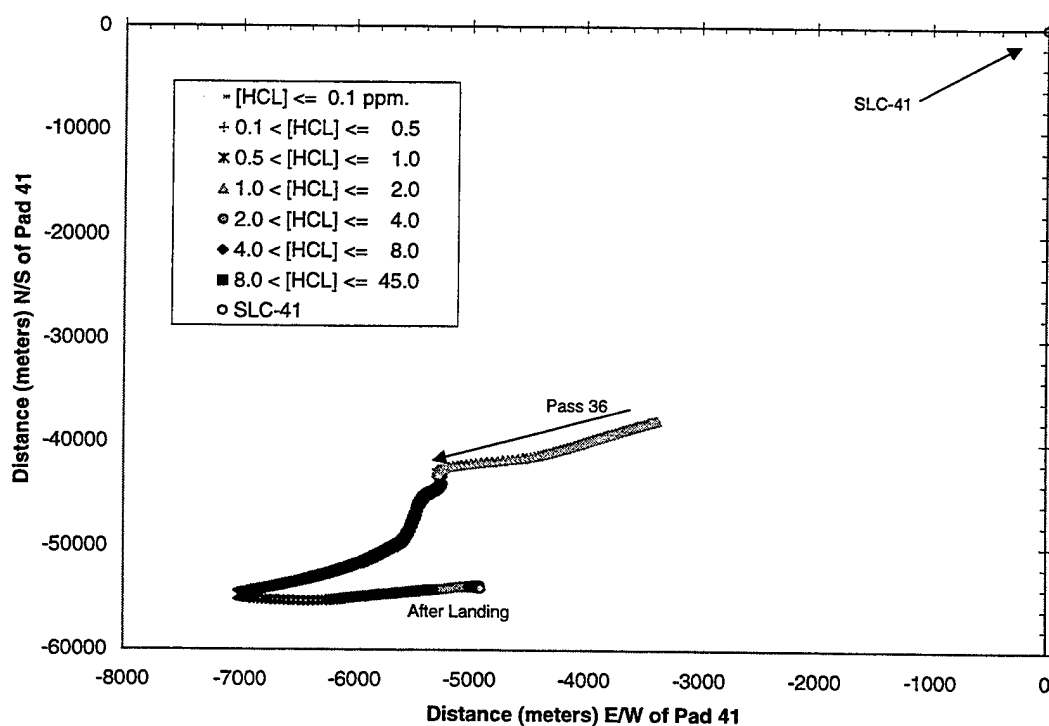
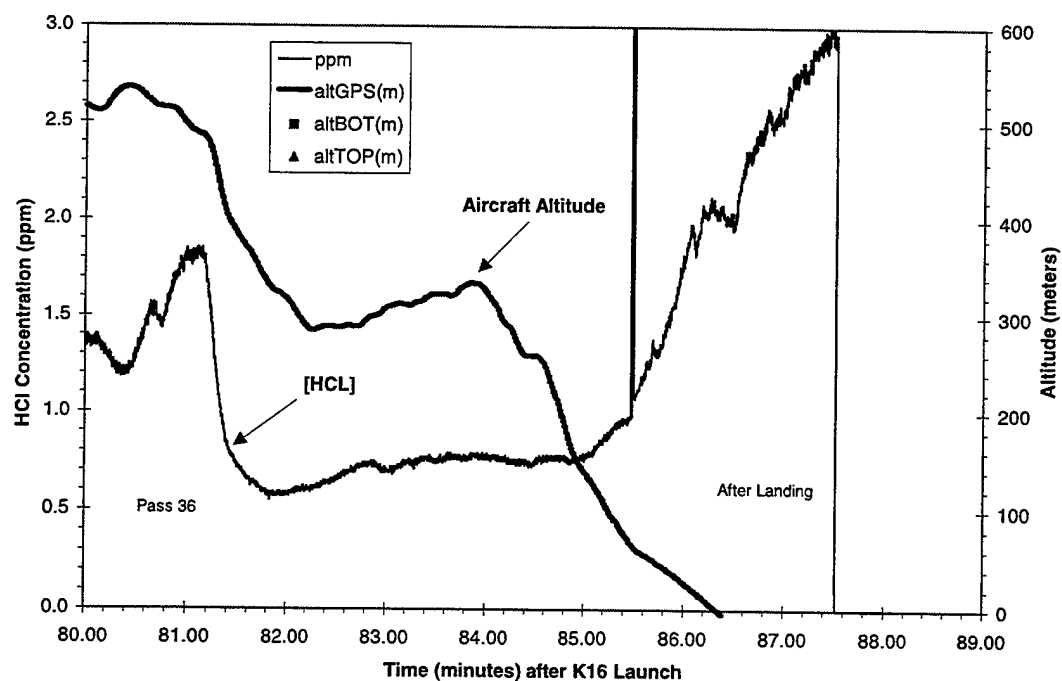


Figure B-9. Time and Cartesian plots for aircraft pass 36 and Runway (T = 80 to 88 minutes).

LABORATORY OPERATIONS

The Aerospace Corporation functions as an "architect-engineer" for national security programs, specializing in advanced military space systems. The Corporation's Laboratory Operations supports the effective and timely development and operation of national security systems through scientific research and the application of advanced technology. Vital to the success of the Corporation is the technical staff's wide-ranging expertise and its ability to stay abreast of new technological developments and program support issues associated with rapidly evolving space systems. Contributing capabilities are provided by these individual organizations:

Electronics and Photonics Laboratory: Microelectronics, VLSI reliability, failure analysis, solid-state device physics, compound semiconductors, radiation effects, infrared and CCD detector devices, data storage and display technologies; lasers and electro-optics, solid state laser design, micro-optics, optical communications, and fiber optic sensors; atomic frequency standards, applied laser spectroscopy, laser chemistry, atmospheric propagation and beam control, LIDAR/LADAR remote sensing; solar cell and array testing and evaluation, battery electrochemistry, battery testing and evaluation.

Space Materials Laboratory: Evaluation and characterizations of new materials and processing techniques: metals, alloys, ceramics, polymers, thin films, and composites; development of advanced deposition processes; nondestructive evaluation, component failure analysis and reliability; structural mechanics, fracture mechanics, and stress corrosion; analysis and evaluation of materials at cryogenic and elevated temperatures; launch vehicle fluid mechanics, heat transfer and flight dynamics; aerothermodynamics; chemical and electric propulsion; environmental chemistry; combustion processes; space environment effects on materials, hardening and vulnerability assessment; contamination, thermal and structural control; lubrication and surface phenomena.

Space Science Application Laboratory: Magnetospheric, auroral and cosmic ray physics, wave-particle interactions, magnetospheric plasma waves; atmospheric and ionospheric physics, density and composition of the upper atmosphere, remote sensing using atmospheric radiation; solar physics, infrared astronomy, infrared signature analysis; infrared surveillance, imaging, remote sensing, and hyperspectral imaging; effects of solar activity, magnetic storms and nuclear explosions on the Earth's atmosphere, ionosphere and magnetosphere; effects of electromagnetic and particulate radiations on space systems; space instrumentation, design fabrication and test; environmental chemistry, trace detection; atmospheric chemical reactions, atmospheric optics, light scattering, state-specific chemical reactions and radiative signatures of missile plumes.

Center for Microtechnology: Microelectromechanical systems (MEMS) for space applications; assessment of microtechnology space applications; laser micromachining; laser-surface physical and chemical interactions; micropropulsion; micro- and nanosatellite mission analysis; intelligent microinstruments for monitoring space and launch system environments.

Office of Spectral Applications: Multispectral and hyperspectral sensor development; data analysis and algorithm development; applications of multispectral and hyperspectral imagery to defense, civil space, commercial, and environmental missions.